Accepted Manuscript

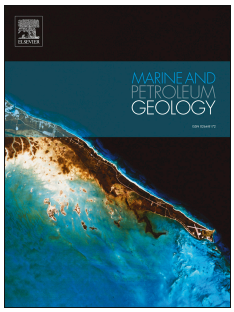

Seismic and structural characterization of fluid escape pipes using 3D and partial stack seismic from the Loyal Field: A multiphase and repeated intrusive mechanism

Daniele Maestrelli, David Iacopini, Ali Jihad, Clare E. Bond, Marco Bonini

PII: S0264-8172(17)30325-2

DOI: 10.1016/j.marpetgeo.2017.08.016

Reference: JMPG 3033

To appear in: *Marine and Petroleum Geology*

Received Date: 19 January 2017

Revised Date: 23 June 2017

Accepted Date: 11 August 2017

Please cite this article as: Maestrelli, D., Iacopini, D., Jihad, A., Bond, C.E., Bonini, M., Seismic and structural characterization of fluid escape pipes using 3D and partial stack seismic from the Loyal Field: A multiphase and repeated intrusive mechanism, *Marine and Petroleum Geology* (2017), doi: 10.1016/j.marpetgeo.2017.08.016.

Seismic and structural characterization of fluid escape pipes using 3D and partial stack seismic from the Loyal field: a multiphase and repeated intrusive mechanism.

Daniele Maestrelli[1,2], David Iacopini [3], Ali Jihad [3], Clare E. Bond [3], Marco Bonini [4]

1) **Dipartimento di Scienze della Terra, Università degli Studi di Pisa, via S. Maria 53, 56126, Pisa**
2) **Dipartimento di Scienze della Terra, Università degli Studi di Firenze, via G. La Pira 4, 50121, Firenze**
3) **Geology and Petroleum Geology Department, University of Aberdeen, King's college, Aberdeen AB24 3DS**
4) **Consiglio Nazionale delle Ricerche, IGG, UOS Firenze, Via G. La Pira, 4, 50121 Firenze, Italy**

Corresponding author: *Daniele Maestrelli, e-mail (1): daniele.maestrelli@for.unipi.it e-mail (2): daniele.maestrelli@gmail.com , Cell: +393297265206*

Abstract

The potential for fluid leakage from sub-surface reservoirs has important implications for CO_2 storage, hydrocarbon reservoirs and water resources. Understanding the genesis, morphology, fluid flow mechanisms and extent of fluid escape from reservoirs allows for better risking of geological resources and storage potential. Here we describe in detail the structures of fluid escape pipes from the Loyal field, observed from a 3D full and partial stack seismic dataset. The seismic imagery suggests that the fluid escape pipes are rooted at least in the main Paleocene reservoir and by-pass the reservoir seal to cross the post Lista Formation overburden up to the intra-Neogene units. The pipes extend for a few hundred meters to a few kilometres and show a varying shape structures from blow-out structures to incipient mud volcanoes. The structural relation of the pipes termination suggest they were active between the formation of Neogene faults and fractures and the erosive event related to the Intra-Neogene unconformity. A detailed analysis of the seismic characteristics observed both from main baseline and partial stack data allows a division of the pipes into two families: (1) seeps and pipes following structural discontinuities (2) pipes unrelated to the pre-existing structural features. The pipes internal seismic response, the reflector termination of the main conduits and the distribution of stacked bright reflectors suggests an upward migration mechanism (during pipe birth and development), requiring a cyclic switching from non-Darcy hydrofracturing (during overpressure) to Darcy flow lateral migration (during low-pressure stage). The improved understanding of the seal by pass

structure affecting the overburden structure will allow for better de-risking of the geological area and improve the velocity model of the overburden in the study area.

Keywords: Fluid escape pipe; mud intrusion; fluid leakage; 3D seismic; Loyal Field; North Sea

1. Introduction and aims of the study

During the last decade, leakage structures (e.g. “fluid escape pipes” or “blow out structures”) have been widely documented globally. These fluid escape pipes have been identified and investigated by means of high-resolution seismic techniques (Davies, 2003; Berndt, 2005; Løseth et al., 2011). Fluid escape pipes can be described as structures allowing the migration of fluids from a reservoir toward the surface, bypassing reservoir seals and cutting the stratigraphic sequence. In many cases fluids reach the seabed. Mud volcanoes and sand injectites are also seal bypass structures (Cartwright et al., 2007) and, even if they cannot be categorised as fluid escape pipes, these structures are responsible for fluid and sediments remobilization. The growing interest in the location, genesis and deformation associated with all these fluid/sediments mobilization mechanisms in the subsurface, is driven by a number of factors: 1) risk to seabed infrastructure from surface deformation; 2) risk associated with oil and gas reservoir seal failure, and consequent loss of hydrocarbons; and associated with the latter 3) the environmental risk of unwanted fluid escape onto the seabed and into the oceans.

These risks are mostly associated to the possibility of a linkage between the reservoir and the seabed, involving the formation of pockmarks (meters to hundreds of meters wide depressions) or craters (resulting from the coalescence of pockmarks, kilometres wide), resulting by the sediment fluidisation and instability in the upper unconsolidated sedimentary layers below the seabed. Furthermore, fluid escape pipes have the potential to drain (partially or totally) a reservoir (Cartwright & Santamarina, 2015), entailing, in the most unfavourable cases, the dispersion of hydrocarbons into the seawater and atmosphere. Moreover, within scenarios of potential subsurface storage volume for wastes (such as CO_2), the effect of fluid escapes pipes on the reservoir integrity must be considered (Bitrus et al., 2016). The establishment of potentially unpredictable subsurface pressure regimes and complex lateral velocity variation is critical in this respect.

Along this line in the last 20 years, the use of high-resolution 2D and 3D seismic datasets to characterise the sub-surface has improved the interpretation and analysis of fluid escape pipe

structures (from source to the conduit). High resolution seismic imaging of fluid escape pipe geometries and distribution, has led to more accurate descriptions of their genetic mechanisms and relationships to surrounding geological features (Davies, 2003; Judd & Hovland, 2007; Cathles et al., 2010; Løseth et al., 2011, Cartwright & Santamarina, 2015). Nonetheless, mechanisms that control their initial genesis are still uncertain, even with the use of improved seismic imaging. These uncertainties stem, in part, from the limits of clear seismic imaging of the internal structure of fluid escape pipes (Moss & Cartwright, 2010). The chaotic nature of the deformed sediment in a fluid escape pipe from the root zone up through the fluid conduit results in poor, incoherent seismic reflections that directly impact the clarity and detail of the seismic imagery (Graue, 2000; Davies, 2003; Cartwright et al., 2007; Løseth et al., 2009 and reference therein; Cathles et al., 2010; Cartwright & Santamarina, 2015).

In this work, a detailed 3D seismic analysis provides a description of a series of fluid escape pipes from the Loyal Field, Scotland. This oil and associated gas field was discovered in 1994 and recently re-developed by a consortium led by BP (Leach et al, 1999). The study aims to contribute to a better understanding of the process controlling the final morphology of fluid pipe escape structures and their triggering processes. We report the geospatial distribution of the fluid escape pipes with respect to other geological features mapped in the seismic dataset following the approach by Lutz (1986), Bleacher et al. (2009), Hustoft et al. (2010), Roberts et al. (2011) and describe the fluid escape pipes variable internal and external architecture using their 3D seismic expression. We explore the seismic response from the main internal conduits using an AVO analysis based on partial stack data. Finally, we propose an evolutionary model for their genesis and development, considering the mechanisms for intrusion through the overburden Paleogene and Neogene stratigraphy.

2. Dataset and Methodology

The 3D seismic dataset used in this work is located in the southernmost sector of the Faeroe-Shetland Trough, on the edge of this channel (Fig. 1), and is referred to as the Loyal Field, situated in quadrants 204/205 of the UKCS, not far from the Judd sub-basin and the Westray Ridge structural high. It covers an area of the subsurface about 15 by 17 kilometres.

The seismic dataset consists of a base line seismic and successive, fully reprocessed, time-lapse surveys acquired to image field development during the production phase (1996-2010). The time-lapse seismic data has been reorganized and released by BP as full and partial stack (near, medium, far). Inverted V_p/V_s , reflectivity volumes were also accessible. The Loyal field seismic

dataset utilized for the analysis is composed of a 3D pre-injection full (1996) and partial stack seismic dataset (acquired from 2000-2010 and subsequently reprocessed in 2010 by Western Geco and CGG companies. Inline-crossline binning is 12.5x12.5 m and the data has been migrated using a pre-stack Kirchhoff depth migration (represented in time domain). Amplitude integrity has been maintained by a variety of weighting functions compensating for geometric spreading and acquisition irregularities. The Seismic dataset is characterized by zero-phase American polarity (red is the wiggle peak). In the area of interest (~4 kilometres depth) the seismic is characterized by a range of frequency varying between 20-80 Hz. According to the Vertical Seismic Profile (VSP) data (Fig. 2h) the average overburden velocity across the area of interest varies between 1700 and 2200 m/s that point to a tuning thickness ($\lambda/4$) varying between 5 and 27 meters.

2.1. Well data

Data from a single well (204/20) with wire line information was provided and utilized to well tie the seismic dataset and characterize the main stratigraphy. Figure 2 shows the interpretation and naming of the main reflective units (the T10 to T36 intervals, where the main reservoir is located, and the Top Lista Formation up to the Top Balder Formation). No stratigraphic information is directly available for the overburden but a VSP velocity information was available (Fig. 2h). For the pre Top Balder units a reflectivity model has been reconstructed using the available sonic and density log (respectively fuchsia and blue curves in Fig. 2b). A simple convolutional model (with an extracted wavelet) was used to obtain the reflectivity (Fig. 2c), and synthetic seismic log (Fig. 2e) to tie the seismic reflectivity model to the well. The main reflectors targeted are the main well top and reflectors T10 to T38. The information was used to reconstruct the root and source of the fluid escape pipe structures.

2.2. Methods

The 3D seismic dataset was interpreted using Petrel® (2016 version) and the major reflectors including the pre-Lista formations were mapped. Interpretation was carried out by manually picking seismic reflections on a line-by-line basis with a grid increment spacing of 2x2 (representing a separation of 25m x 25m) on inlines, crosslines and using arbitrary lines when required. The seismic interpretation approach aimed at the definition and characterization of pipes and other leakage structures (faults and fractures), focusing on the pipes and their relationship to mapped faults and fractures as well as on their geometry. In order to improve the

visualization of the edge and enhance amplitude variation of the picked reflectors, two specific attributes were used: the Variance and the Root Mean Square (RMS) amplitude attributes. A relative analysis of the amplitude across the near medium and far offset stack dataset and an estimate of the related gradient and intercept values has been also been performed using parser functionality of Geoteric® (ffA).

2.2.1. Attribute analysis

To improve the quality of our interpretation we made use of various seismic attributes, particularly the Variance volume attribute and the Root Mean Square attribute (RMS).

The Variance (Chopra & Marfurt, 2007) can be seen as the lateral counterpart of amplitude analysis as the later indicates vertical variations. It has been used with the aim of better visualizing the 3D fault pattern observed in the dataset.

The RMS (defined by Taner et al., 1994) represents a post-stack attribute that computes the square root of the sum of squared amplitudes divided by the number of samples within the specified window used. A positive anomaly in the RMS value could, among other things, be correlated with fluid presence. However, RMS is sensitive to noise and consequently it is only partly related to the relative post stack amplitude value (e.g. Brown, 2011).

2.2.2 Methodology for pipes structural analysis

We quantify the 2D-3D pipe geometry, by measuring sectional axes length, their ratio (long/short) and the length of the investigated pipes.

Sectional axes: In order to determine axes variability and pipes ellipticity the axes are measured in two different directions by using the seismic volumes inlines and crosslines. In order to appreciate the vertical variability of the pipe conduits we chose to measure the axes length always across two cross sections and at two different heights, corresponding to the height of the Top Lista Formation and at the pipe termination or “terminus”.

Axes ratio: In order to identify pipe geometry (circular vs elliptical plan view shape), we calculated the ratio between the long and short axes measured along the inline and crossline directions. This ratio is referred herein to as “apparent aspect ratio” (AR_A). Given that inlines and crosslines do not

necessarily correspond to the actual maximum and minimum axes of a pipe, the obtained apparent aspect ratio (AR_A) is only an approximation of the actual pipe elongation, and therefore it cannot be used for correlation with the regional stress field. Nonetheless, the AR_A values are still effective in recognizing the presence of non-circular pipes (i.e. AR_A is often >1). It is noteworthy that it was not possible to measure axes for each pipe, due to the fact that in some cases the average value was not representative of the geometrical variability along a pipes conduit and thus a single axis measurement was not deemed to be meaningful. In some specific geometrical end-member case, the pipes shows strongly irregular, coalescent and/or interacting shapes and therefore the axes length were not taken into account.

Length: Another significant parameter used for the pipe characterization, is their length (measured from the root to the pipe terminus) although it is not a parameter easy to measure. This is mainly due to loss of coherency in the seismic signal with depth, which in the case of pipe structures is augmented by the presence and passage of fluids disrupting previously reflective strata. This poses strong uncertainty in the definition of the source zone of the pipe. The pipe terminus (i.e. the upward termination of a pipes structure; Cartwright & Santamarina, 2015) is instead often easily detectable and mapped in the seismic image data.

2.2.3 Methodology for pipes statistical analysis (two points statistic)

In an effort to verify possible relations between the pipes and the mapped faults, a “two-points azimuth statistics” (Lutz, 1986; Bleacher et al., 2009) approach was applied to our dataset. This method was used with success in mud volcanism settings to analyse vent alignments, distribution and their dependence on mapped structures (Roberts et al., 2011). Distance and azimuth were measured for each pipe with respect to all the other pipes (from east to west, to avoid the repetition of measurements). The main target was to obtain classes of azimuth frequencies able to determine if the pipes show preferential alignments.

2.2.4. Amplitude analysis across partial stack

Anomalous amplitude versus offset (AVO) behaviour is widely recognized as an important aid to lithology and fluid prediction (Castagna, 1993, Castagna & Swan, 1997). Specifically within clastic sequences, it can distinguish the fluid content within a defined reservoir and help the interpreter

to infer the petrophysical meaning of the signal response. From a physics point of view the amplitude versus offset analysis makes use of the following Shuey linear approximation of the Zoeppritz equation (1)

$$R_i = R_0 + G\,Sin^2 i \qquad (1)$$

The equation relates the p-wave reflection coefficient R_i at a specific angle of incidence *i* to the zero offset intercept R_0 and the AVO gradient *G* (that depends on the Poisson ratio). In order to obtain information related to the R_0 and *G* parameters the interpreter needs to access a pre-stack common depth point gathers position at different distance (*i*) (or offset) respect to the source. If not available, the partial stack reprocessed (using amplitude preservation workflow) may be used to obtain average value of the AVO attributes at three different range of offset (the near, medium and far). In this study we could rely on a quantitative amplitude analysis performed using the far, medium, and near partial stack.

Re-arranging the linearized Shuey equation (eq.1) for a partial stacks, we obtain the following gradient values:

$$Gradient = \frac{R(\theta f) - R(\theta n)}{\sin^2 \theta f - \sin^2 \theta n} \qquad (2)$$

$$Intercept = R(\theta f) - Gradient * \sin^2 \theta f \qquad (3)$$

Where $R(\theta_f)$ represents the reflectivity measured at the far offset θ_f, and $R(\theta_n)$ the reflectivity measured at near offset θ_n. Therefore, as by equations "2" and "3" the near medium and far partial stacks allow us to qualitatively describe the amplitude variation through offset within selected offset. Our dataset allowed to select partial stack at 10 degrees distance and to estimate the gradient and intercept values. A cross-plotting of the calculated gradient and intercept values will then be used to explore the petrophysical trend.

Before using the partial stacks a number of workflows to ensure quality control of the amplitude, phase, frequency and bedform alignment between the partial stacks volumes has been applied (Ross & Beale, 1994). Misalignment of stacks can in fact lead to false positive AVO anomalies or false 4D/multiple volumes interpretations. Thus being able to identify those undependable areas can help to increase the confidence on the multi-volume analysis. The partial stack data analysed and used for those amplitude analyses indicated a good phase, amplitude, frequency and bedform correlation excluding significant mis-alignment in the area of interest.

3. Geological framework

3.1. Tectonic and structural framework

The dataset is located in the Faeroe-Shetland Trough (Fig. 1a,b,c) a channel covering about a 400 kilometres long and 175 kilometres wide area (Ritchie et al., 2008), that divides the Faeroe Platform (the continuation of the Iceland Faeroe Ridge), from the westernmost portion of the European continental shelf, represented in the area by the Shetland Platform. The trough reaches up to 1300-1400 meters in depth in the southernmost portion and is associated with a series of minor satellite basins and sub-basins (Fig. 1a,b, and Fig. 3a,b; Sørensen, 2003; Ritchie et al. 2008).

The geology reflects the complexity of the evolutionary history of the Faeroe-Shetland Trough (e.g. Doré et al., 1997, 1999; Dean et al., 1999, Roberts et al., 1999): after erosion and extensional collapse of the Silurian Caledonian orogeny during the early Palaeozoic, a major phase of rifting occurred in the area during the Mesozoic-Early Cenozoic. The opening of the North Atlantic Ocean was followed by eruption of basaltic lavas in the area, and was associated with a new phase of subsidence during the Early Eocene, representing the final phase of continental break-up (Sørensen, 2003). Overall, the crustal stretching due to these extensional tectonic phases is responsible for the shallow Moho (16 kilometres depth) now imaged by reflection seismic profiles beneath the trough (Richardson et al., 1999, Smallwood et al., 2001). Thereafter, four major compressional phases active during the Eocene, Oligocene, Miocene until the Pliocene, were mostly responsible for major tectonic inversion of basement rift structures. This complex sequence of tectonic events led to the formation of a major physiographic element, the Faroe-Shetland channel, which can be subdivided into a series of structural highs, showing a predominant NE-SW orientation, and related sub-basins (Sørensen, 2003). With reference to the quadrants of interest 204/205 (the location of our seismic volume), the main structural elements observed (Fig. 1b) are

the Mesozoic/Paleozoic Judd High (in the south-westernmost portion of the area), which is connected with the Judd sub-basin by the Judd Transfer Zone; the Westray Ridge, running approximately SSW-NNE; the Flett Ridge, and the Rona Ridge, which strikes approximately NE-SW and is cut by the Westray Transfer Zone. The West Shetland basin, in the southeast of quadrant 205, is bounded by the Shetland Spine Fault. Ritchie et al. (2008) present (Fig. 1b) structures related to the Cenozoic compressional phases as follows:

- the E-W- trending Judd anticline, located north of the Judd structural high, a 33 kilometre-long anticline developed by the Early Eocene and late Oligocene compressional phases.
- the South Judd anticline, a short (18 km) asymmetrical NW trending growth fold, probably developed during a single (Early Oligocene) tectonic phase.
- the 45 kilometre-long Westray anticline, which is located in the Judd sub-basin close to the Westray lineament runs parallel to the South Judd anticline (thus has a NW trend), crosses the Westray high. It is the result of three distinct compressional tectonic phases (Early Eocene, middle Eocene and probably Pliocene).

All the structural highs were widely influenced during their evolution by the presence of the Westray and the Judd lineaments, which have been both reactivated accommodating deformation transfer between faults (Ritchie et al., 2008).

3.2. Main stratigraphy

In the Loyal Field and surrounding areas, the Cenozoic stratigraphy (Fig. 1d) is composed, from bottom to top, by the T10-T20 sequence (using the BP unified biozonation reference), corresponding to the Ekofisk and Maureen Formations, and the T30-T50 sequence, which hosts the hydrocarbon reservoirs and is represented by the Lista, Sele and Balder Formations (Leach et

al., 1999; Fig. 1d). It is worth noting that the flood basalts erupted during the spreading phases do not affect the Loyal field area (Fig. 1b). Southward to the basalt deposition limit, the continuation of the top of the basalt reflectors laterally corresponds to the Top of Paleocene sediments, which are represented in the study area by the T38-T40 succession (Sørensen, 2003). These horizons are represented by the Top of the Lista Formation (Selandian to Thanetian) which acts as major seal for the underlying hydrocarbon reservoirs (Fig. 1d). On top of this sequence, younger units are mainly represented by turbiditic channelized sediments and contouritic deposits of Mio-Pliocene age (Fig. 3a). We tentatively correlate our dataset with the interpreted seismic lines described by Stocker et al. (2002), one of which cuts the Faroe-Shetland Channel and runs parallel to the crossline direction of the Loyal field seismic volume close to the study area (Fig. 3). Stoker (1999) and Stoker et al. (2002) described the post Eocene stratigraphic sequence of the Faroe-Shetland Channel as built up by the units of the Westray and Norland groups (Fig. 3c). The latter is characterised by the presence of three major unconformities (Fig. 3b and c): the Latest Oligocene/Early Miocene Unconformity (LOEMU), the Intra-Neogene Unconformity (INU, Latest Miocene/Early Pliocene) and the Glacial Unconformity (GU, of Middle Pleistocene age), dividing the group into the Lower, Middle and Upper Norland Units (Fig. 3c). However, due to the lack of core and well top data for the Neogene section, a precise correlation of the main observed unconformity to either the LOEMU or INU is still uncertain.

4. Results

The Loyal Field 3D dataset provides an opportunity to analyse seal bypass structures, widely distributed in the whole area covered by the seismic. In the description of these leakage structures, we refer throughout the following section to the term “pipe” or “blow out structures” with a general descriptive and not genetic significance (Cartwright & Santamarina, 2015. For an in-

depth analysis of pipes variety and genetic mechanisms see Cartwright et al., 2007; Løseth et al, 2009; Cathles et al., 2010; Moss & Cartwright, 2010).

4.1. Preliminary considerations: insight into the Loyal Field seismic volume

In order to understand the tectonic and sedimentary setting we give a general overview of the entire seismic, describing the major structural characteristics of the seismic volume.

4.1.1 Deep faults and seal interaction

Three-dimensional mapping of the large-scale structure helped to recognize the main rift fault pattern (Leach et al., 1999), with an orientation roughly E-W, (Fig. 4a) partially sealed by a package of Paleocene sediments identified by high-impedance reflectors that correspond to the top of the Lista Formation (Selandian-Thanetian, Fig. 4a). Except in some rare cases, the main rift faults do not cut the horizons at the top of and above the Lista Formation (Fig. 4a). These layers are key-horizons as they correspond to the seal of the main reservoirs (the Loyal Field corresponds to the T35 BP Unit or the Glamis member of the Lista Fm. in Figure 1d, representing a sandstone package, Leach et al., 1999) and their continuity therefore enables accurate three-dimensional mapping of the seal.

4.1.2 The seal reflector

When analysing the surface derived from mapping the seal reflector, two main features are observed (Fig. 4b): the horizon is gently sloping toward the N-NE, and its inclination increases in the north-easternmost corner of the study area. The south-western sector shows a buried topographical high running approximately E-W. Further, the Top of the Lista Formation shows an irregular surface geometry, from the presence of mounds of variable shape, from circular to elliptical, or strongly elongated along one axis. Mound alignments are identified (MA in Figure 4b).

4.1.3 From the seal to the seabed

Channels are interpreted in the upper part of the seismic volume, above the seal reflector: frontal and lateral accretionary seismic facies (LAP's) are well developed in proximity to the seabed, where contourite sediments (already well documented in West Shetland by Stoker et al., 1998) were deposited during the Mio-Pliocene (Fig. 4c). Surprisingly, on the seabed surface, evidence of fluid leakage such as pockmarks are rarely detected. Only some scours, up to a few kilometres long and hundreds of meters wide, are visible in the southern sector of the study area. Such features, are interpreted in other areas of the North Sea as iceberg plough marks (e.g. Judd & Hovland, 2007; Dowdesell & Ottesen, 2013; Knutz, 2010), and presumably formed during the last glaciation (Fig. 4 d).

4.2. Seismic *characterization of fluid escape pipes in the Loyal Field*

We describe in the following sections the interpretation of the fluid escape pipes seismic expression, carried out using the information derived from the general geological analysis shown in Section 4.1.

4.2.1. Fluid escape architecture

High-resolution seismic imagery allowed a detailed investigation of the leakage structures affecting the overburden above the T36-38 units. More than fifty pipes were mapped and analysed for their characteristics: their geometry, internal structure and seismic expression. Some examples are reported in Figures 5a and 6. The Top Lista Formation horizon consists of a mudstone package (Sørensen, 2003) acting as a seal layer (Leach et al., 1999). It may have be

responsible, during the Eocene-Miocene compressive activity, for the fluid pressure, and may have played an important role in the formation of the pipes. The pipes are deeply rooted (more than one kilometre; see the R-TL segment length described in Fig. 11) beneath the Top Lista, and display variable shapes to the pipe flanks (Fig. 5a, as described also by Cartwright & Santamarina; 2015; Løseth et al; 2011). Focusing on the roots, some of them are isolated, columnar and straight (pipe "P2" in Figure 5a, cf. Cartwright & Santamarina, 2015), while some others are coalescent or show a variable geometry (respectively pipes "P1" and "P3", "P4" in Figure 5a, cf. Cartwright & Santamarina, 2015; Løseth et al, 2011). Above the Top Lista Formation, the pipe conduits show variable geometries, from straight columnar shapes (Fig. 6b), to diffuse structures with poorly defined boundaries (Fig. 6c). The source zone of these pipes is difficult to identify, due to the low amplitude and poor resolution of the seismic signal. In order to minimize this problem an additional Automatic Gain Control (AGC) has been applied to the stacked seismic (e.g. Fig. 4a). The AGC attribute was used for a better identification of the described rift fault pattern, represented by listric normal faults, composing a system of tilted fault blocks. The portion of the volume affected by the main rift faults is located within the Loyal field reservoir and the faults are sealed by the Lista Fm. In this area, hydrocarbons are present in the root zone of the pipes (Leach, 1999) and (as the AVO suggests, see section 4.2.5) they were possibly part of the fluid mixture that flowed through the pipe conduits. During their upward propagation, the pipes invariably cross the Top Lista Formation (see Figure 5b, 6b,c and d), enhancing a series of mounds widely distributed and clearly detectable at the level of this surface (Fig. 4b) but also above it (Fig 7a).

4.2.2. Internal conduit architecture

The pipes observed and mapped show also a variable internal seismic expression along the conduit. While some of them appear straight and well defined in their shape, other pipes do not

show sharp well defined boundaries, but are identified by continuous bright anomalies through stacks of horizontal reflectors (Fig.8a). The variation within their lateral extent suggests the pipes probably experienced lateral migration of fluids resulting in strongly irregular pipe shapes (Fig. 8a). In other cases, we observed that more than one pipe interacted, resulting in coalescent structures (Fig. 8b). A major feature of the pipes conduit is the upward convex deflection of the main seismic horizons, which are imaged along the pipe length for most of the conduit structures (Fig. 6a,b). This horizon deflection has been observed, except in some rare cases, in most pipes, with different degree of development. In some of the largest examples, a chaotic expression of the seismic signal is visible: the reflection terminations of the deflected horizons show a clear loss of amplitude and a disruption of the internal architecture of the pipe (Fig. 5b). Across the narrowest pipes (Fig. 6b,d) this chaotic feature is not visible and the upward deflection of the horizons is variably reduced along part of the conduit (Fig. 5b), or the reflector appear simply deflected and characterized by a loss of amplitude (Fig. 6d). The widest pipes show a thickness wider than the horizontal seismic resolution, hence the imaged internal pipe architecture (Fig. 6b and c), can be considered as unaffected by artefact seismic imaging (Løseth at al. 1999). In other cases the pipe conduit shows a rather broad geometry (Fig. 6c) suggesting a diffuse seeping of fluid from the pipe into the surrounding strata but with no deflected horizons. Rare or no pinching out geometry of single reflectors (or seismic truncation sensu Plaza-Faverola et al., 2011) are observed across the fluid pipe boundary walls. Depending on the frequency and velocity distribution, Moss & Cartwright (2010) suggest 100 meters as the threshold width for clear seismic imaging of the internal architecture of fluid escape pipes. In our case, we register often a constant upward deflection in the horizon termination of wide pipes with diameters greater than 100 m. This allowed to perform an amplitude analysis across some selected fluid pipe rocks. According to seismic theory, and to well documented seismic pipe architectures (e.g. Moss & Cartwright, 2010; Cartwright &

Santamarina, 2015), the presence and the passage of hydrocarbons or mixed fluid, due to their lower impedance contrast, should lead to a "push down" and/or amplification of the horizons rather than an upward deflection. The fact that not all fluid escape pipes are affected by upward hooking suggest that they are not the effect of widespread velocity artefact. Therefore, all the above observations support the idea that the reflector geometry observed represents the real internal architecture of the pipes, the result of pipe genesis and the flow of material in the pipe. When possible, we considered the inflection point in the horizon deflection as the pipe boundary for our measurements of length and diameter (see following section).

4.2.3. Pipe architecture: diameter and length

We quantified pipes geometry as explained in section 2.2.2 and we here report the measured diameter values (Fig. 9). The diameters vary between 60-80 metres and 300-350 metres, with some outliers reaching 580-600 metres. In most cases, the diameter measured at the pipe terminus shows a lower value than the diameter measured at the level of the Lista Fm, indicating an upward decrease of the pipe diameter. In other cases this variation is absent and the fluid conduits appear straight. Measured pipe diameters are comparable with previous estimates obtained from seismic data (Cartwright & Santamarina, 2015), as well as with those mapped from exhumed feeder mud volcano conduits (Roberts et al., 2010).The eccentricity (AR_A, Figure 10) indicates that conduits vary from circular ($AR_A \approx 1$) to strongly elliptical ($AR_A >> 1$).

Finally, we measured the length values (measured on seismic inlines) for the analysed pipes (Figure 11). The Top Lista Formation surface (which is invariably crossed by the pipe structures) was used as a "reference position", with the total pipe length measured in two segments: the "Root-Top Lista" (R-TL) and the "Top-Lista-Pipe terminus" (TL-PT), and the two values are then

summed. We used the Vertical Seismic Profile (VPS) available from well log (see Figure 1c for well location and Figure 2h for the VSP curve) to extrapolate averaged velocities V_1 of 1724 m/s and V_2 of 2207 m/s for the TL-PT and R-TL segments, respectively. This allowed us to gain a time-to-depth conversion for the pipe length. As shown in Figure 11, the length values depict the presence of different families: most of pipes reach 600-1000 meters in length, but there are also pipes reaching ca. 1600 metres (or more). These values show that fluid escape pipes as leakage structures are significant structures, some of them constituting a deep rooted link between the reservoir and the shallow subsurface (cf. Tab. 1 in Cartwright et al, 2007). With the same time-to-depth conversion (using the velocity V_1), we also measured the distance between the pipe terminus and the seabed surface (PT-SS segment in Figure 11). The pipe terminus was mapped at the top-end of the horizon upward convex deflection. Using this criterion most of the pipes terminate a few meters or hundreds of meters below the seabed (150-250 meters up to 500-550 meters). In particular, the majority of the pipes terminate beneath a visible package of horizons interpreted as an erosive unconformity overlying a lateral or frontal accretionary package deposited in fluvial channel bodies (Fig. 5a). Other pipes terminate beneath this surface at a range of different depths.

4.2.4. Evidence for intrusive dense material coupled to fluid

In order to investigate the type of fluid driving the upward propagation of the pipes, we describe the pipes structure and their internal signal response. At many pipe terminus we observe amplitude brights (Fig. 6a) that extend laterally away from the conduits (see section 4.2.5). In some cases it was also possible to identify amplitude anomalies above pipe structures (see pipe "P4" in Figure 5a). Furthermore, the terminus of some pipes show a buried pockmark (Fig. 6b and d), suggesting of sediment collapse due to emission of fluids at a paleo-seabed. These indicators

may account for the presence of a water/hydrocarbon mixture. Nonetheless, as mentioned before the majority of the pipes show a marked deflection of the horizon toward the surface (see for example the pipes in Figure 5a and 6a,b, and description above, marking the boundary of the pipe). In Figure 5b, a detailed example of horizon upward convex deflection is shown: the disrupted pipe conduit is bounded by upward deflected seismic horizon. No magmatic intrusive structure (responsible for higher velocity) have been observed in this area and therefore we do not assign those deflection to a pull up velocity effect. When we focus our analysis to the terminus zones, the horizons clearly show that they are subject to progressively less deflection with respect to the deeper horizons and to the pipe root (e.g. pipe "P1" in Fig. 5a,b); this may imply a progressive decrease in the fluid seepage forces. It is this particular geometry that may indicate the presence of a more complex fluid mixture. The relative dominance of the effects of horizon architecture (forced upwards by fluid expulsion) and the seismic response of a rock saturated in a water-hydrocarbon mix needs to be considered during the interpretation of those observations. We will discuss further this evidence.

4.2.5. Lateral versus vertical flow migration using partial stack

Analysis of amplitude across different offsets of the partial stacked seismic dataset provides additional insight about the nature of pipe propagation and fluid type. In our case three selected cropped volumes (reprocessed following an amplitude preservation workflow) showing the near, mid-, and far-offsets stack, were used to visualize selected pipes internal geometry (Fig. 12) from the different seismic signal responses of the datasets (Ostrander, 1984). In Figure 13a to 13c we represent the trace equivalent response of the amplitude anomaly marked by white ellipse in Figure 12, while in Figure 13d to 13f we calculate the seismic envelope of the trace. The three figures clearly indicate the following aspects:

- The distribution of bright anomalies along specific horizons testifies to the presence, and lateral propagation, of fluids along specific seismic horizons. It also suggests that fluid migration is by Darcy Flow, exploiting paths with favourable effective permeability.
- From the near- to the far- offset the bright amplitudes decrease their relative amplitude (we refer to this seismic behaviour as a "normal trend). The "normal trend" amplitude suggests that the fluids are "non-hydrocarbon bearing".

A "quasi-inverse trend" (i.e., increasing bright amplitude in the near- to the mid-offset seismic datasets) is instead visible at the pipe terminus (Fig. 12a,b,c, red dashed circle). The zoomed view of the envelope (Figure 13g to 13i, marked by the arrow) highlights the increasing amplitude response from near to mid offset and then relative decrease for the far offset. It suggests the presence of fluid possibly containing some hydrocarbons. To test these observations we calculated the gradient and intercept values of those anomalies and plotted their values into a gradient/intercept diagram. Due to the sandstone-mudstone nature of the units we assumed the clastic sequences amplitude anomalies bearing proposed by Rutherford petrophysics analysis (Rutherford & William, 1989) (Fig. 13j) and used the Castagna & Swan diagram (1997) to interpret the cross plot values.

In Figure 13k we plotted the gradient and intercept values of the amplitude anomalies observed in Figure 13a,b,c and calculated using equations "2" and "3". The values indicate the amplitude are consistent with a "class I" and slightly touching the "class IV" of brine and oil bearing sandstones.

Figure 13j suggest the anomalies and trend from Figures 13d to 13f are matching the fluid brine rich class I and IV with some possible oil component. The two results suggest that for the specific amplitude anomalies investigated the hydrocarbon component is not playing a major role in the seismic expression and trend.

4.3. Fault and fracture patterns

Our structural analysis mainly focuses on the post Paleocene fault and fracture pattern, which appears to be associated with the leakage structures. The distribution patterns of the faults and the fluid escape pipes can be spatially interpreted using time slices of the seismic volume. Visualisation of the seismic volume using attributes such as Variance (Fig. 14a,b) enhance the structural pattern of the fault traces which are commonly organised into "horst and graben" systems, as evidenced by the 2D time and depth section analyses. The imaged structures indicate both the presence of normal faults with vertical decametric throw, and fractures with no detectable displacement (Fig. 15a). Their orientation varies over a quite wide range, with three major clusters: E-W, NE-SW, and NW-SE (Fig. 14c). The geometries visible in 2D time slices visualised using the Variance attribute, along with 3D interpretation, may suggest that these structures are similar to polygonal faults (Berndt et al., 2003; Cartwright 1994; Cartwright & Dewhurst, 1998), based on the following considerations: (i) the faults show limited vertical displacement, (ii) the fault trace pattern visible in the time slice view mimics the polygonal faults reported in the North Sea (e.g., Cartwright, 1994; Cartwright and Dewhurst, 1998; Hansen et al., 2005; Cartwright, 2007), and (iii) the structures appear to be mainly contained within the Eocene-Oligocene succession (Fig. 15a). In fact, they rarely cross the Top Lista Fm. and never reach the seabed, their maximum upward propagation sealed by a major unconformity. This unconformity cuts, abruptly, some faults and shows some inflection in graben depressions (Fig. 15a). This suggests that faults may have formed previous to the unconformity, when the corresponding seismic horizons probably represented a paleo-seabed. This is in agreement with the formation mechanisms of polygonal faults, which are thought to develop during early-burial, formed by the dewatering of fine-grained mudstone, in the first few meters beneath the seabed (Cartwright,

1994, Cartwright & Dewhurst, 1998, Cartwright et al., 2007). Furthermore, these major fault systems seem to be associated with fluid migration, as highlighted in time-slices of the RMS attribute (Fig. 15b), in which major structures are seen to propagate from mound like structures at the level of the Top Lista Fm. The mounds are located in the centre and northern sectors of the area, and link to the fault tectonic features as shown in Figure 15a and b. There are no "pipe-like" vertical structures associated with these mounds.

4.3.1. *Pipe azimuthal distribution using two point-statistics*

The aim of this analysis is to generate classes of azimuth frequencies in order to determine if there is a preferential distribution of the pipes (e.g alignments). Pipes distribution is shown in Figure 16a. The probability for a pipe to be aligned with another following the same structure is strictly dependent on their separation distance (the further away they are, the less the probability of correlation). Therefore, frequencies are weighted by multiplying each measurement for a correction factor (ranging between 1 and 10), proportional to the pipe distance and normalised by using the maximum distance observed between two pipes (the multiplying factor is 10 for the two closest pipes, while it is 1 for the two furthest). In Figure 17 the results are expressed through rose diagrams of azimuth frequency. Comparing the weighted frequencies for the whole pipe dataset (Fig. 17c) with the strike orientation of the mapped faults (Fig. 17a), a good correspondence between the main NE-trending peaks is observed, while the minor frequency peaks show some discrepancies. Even if some peaks are reduced by the weighting procedure (compared with the non-weighted dataset, Fig. 17b), some frequency classes are still predominant (e.g. the N-S class is represented by a small peak in the fault distribution of Figure 17a, while in Figure 17c the peaks corresponding to the 70°-90° orientations are small).

We further subdivide the pipes located above the anticline, referred to as “Southern (anticline) cluster”, from those not located above the anticline (“Northern cluster”; Fig. 17e). The “Southern (anticline) cluster”, reported in Figure 17d, shows a greater correspondence to some trends. In particular, the 60°-70° and 120°-130° classes are characterised by higher frequency peaks. This result highlights a correlation between the fault and fracture trends and the pipe alignments in this area suggesting there is a possible dependence of their distribution on these structures. Using to the fact that the closer pipes are the more likely they are correlated, we therefore considered pipes located at variable distance, but excluding every pipe pair below certain threshold distance. This allowed to explore the potential biases of the alignment from the relative distance between a pipe pair. For our purposes we have filtered the pipes used for the analysis by selecting five threshold distances in the range of 1-5 km (our maximum windows of analysis), with an increment of 1 km. We therefore obtained five graphs showing frequency peaks for the azimuth classes for pipes grouped according to this distance. For thresholds ≤2 km, the 110°-140° azimuth classes appear to be more pronounced (Fig. 17i,j) while for thresholds ≥2 km the size of the peaks of the azimuth classes is roughly constant showing two main orientation but not including all the pipe structures. Very close pipes are also presumably associated with sub-seismic fracture trends sub-orthogonal to the anticline axis.

5. Discussion

5.1. Fluid versus solid material intrusionThe Loyal Field contains a series of structures acting as paths for the upward migration of fluids from a deep reservoir (2100-2400 metres below the present seabed) to the palaeo-seabed. Geometrical analysis of the structures highlight that they can be considered as medium- to large-scale pipes developed from a deep source rock that cut through ca. 2 km-thick stratigraphic sequence. Bright amplitude anomalies are interpreted as

evidence of fluids (Ostrander, 1984) propagating toward the seabed from the pipe conduit. AVO analysis on pre stacks suggest that the fluid content is driven by brine rather than hydrocarbon. Fluid migration can occur through the connected pore space in a rock. Nonetheless, the most interesting observed features are the pipe boundaries and internal architectures, characterised by partial internal disruption and deflection of seismic horizons upwards toward the surface (Fig. 5a,b and 6a) that cannot be related with a push up effect of the seismic horizons, due to the low impedance contrast of brine-hyrdocarbon fluid. To interpret the overall pipe geometry and their internal architecture observed (upward deflection, lack of clear push down effect, linked to bright amplitude anomalies) a fluid mixture with a dense component able to deform the pipe flanks during fluid migration, in a similar way to salt or mud diapirism, needs to be taken into account. We therefore hypothesise that the pipes develop from the rising of a dense sediment-fluid mix bearing a hydrocarbon fraction, partly driven by exsolved gas (Brown, 1990). Interestingly, sediment remobilization has been described in the whole North Sea (see below), particularly sand and mud intrusions (salt is excluded, as it is not observed in the area) and related to a major Eocene-Miocene event (Sørensen, 2003). Therefore, some considerations can be done on the nature of the solid fraction of the mixture. Intrusive sand bodies are documented in the North Sea and in the Faroe-Shetland channel (e.g. Huuse & Mickelson, 2004; Shoulder & Cartwright, 2004). These features are originating from mobilization and injection of sediment during the burial process. However, the shape of interpreted sand injectite structures is that of an inverted cone, leading to apparently V-shaped intrusions when observed in 2D sections, with no horizon deflection. This is not observed in our dataset. Therefore, sand-diapirism can be excluded as the main cause of the pipes interpreted here. Mud injections, at a range of scales, have also been widely documented in seismic data over the last decade across the North Sea, as well as in different, and similar, tectonic environments all over the world (e.g., Graue, 2000; Stewart &

Davies, 2006; Cartwright et al., 2007; Løseth et al., 2009; Cartwright & Santamarina, 2015). In particular, small scale mud injections have been reported and named "Type A" by Hansen et al., (2005, cf. mounding in our Fig. 4a and the features shown in Fig.11a in Hansen et al., 2005) in the Norwegian offshore, and are considered responsible for the mounding, but not failure of seismic sealing horizons. In our case, these features do not always appear to be located, as reported by Hansen et al. (2005), at the tip of deeper faults (see Fig. 4a) acting as fluid migration paths. Besides, also large scale mud injection, or better mud volcanoes are widely present in the North Sea. In particular, the Faroe-Shetland Channel, has large mud formed anticlines present in its northern sector (Lamers & Carmichael, 1999; Ritchie et al., 2008). These features developed when the Upper Cretaceous-Early Paleocene sediments (T10) were mobilised during Paleocene tectonics causing a phase of instability. Cartwright et al. (2007) summarise mud intrusions geometries from a range of localities as cylindrical bodies up to ten kilometres long, with amplitude anomalies distributed around and inside the conduit. Furthermore, examples of relict mud volcanoes are reported, showing burial of extrusion cones on the paleo-seabed, overlain by younger sediments (Stewart & Davies, 2006; Cartwright et al., 2007). Hansen et al. (2005) report similar features in the Norwegian margin, named "Type B" structures, described as mud intrusions and showing an internal texture similar to the pipe structures mapped here (cf. our Fig. 5a,b and Fig.13 in Hansen et al., 2005). AVO analysis across some selected large fluid conduit confirm the content of brine sand (Figs 13i and j). Therefore, we propose that the nature of the solid fraction in the fluid-mix consists of fluidised mud and possibly brine sand, creating, in some cases, pipes resembling "Type A and B" structure of Hansen et al. (2005) and possibly creating mud cones at a paleoseabed.

5.2. Pipes alignment and structural control

The plan-view visualization of major faults and pipes (Fig. 16) and the proposed statistical analysis of their distribution (Fig. 17a to 17e), suggest that there is not a correlation and alignment across the whole dataset (Fig. 17e). The faults show a cluster distribution in the central-northern sector of the area unrelated to the main tectonic rift event (Fig. 16 and Fig. 17a,e) and to any tectonic Neogene event, while the main pipe conduits are instead mainly localised in the south, on top of the buried Lista high, which likely consists of a broad anticline. In the northern area, the fluid pipe structures mapped and observed (Fig. 16) are mostly unrelated to the polygonal fault clusters. In the SW sector of the area as suggested by the two point statistical analysis the pipes are aligned to the 120°-140° and 30°-50° azimuth classes that are roughly orthogonal and parallel to the broad SW anticline structure (Figs. 16 and 17a) no matter the threshold of pipe spacing. For thresholds ≤2 km, the 110°-140° azimuth classes show a more pronounced peak (Fig. 17i, j). This can be related to the fact that the pipes in this area are presumably associated with small-scale fracture system still with a trend sub-orthogonal to the anticline axis. A similar correlation between anticline related structural trends and mud/fluid emission has been observed in other regions, and suggests that mud volcanoes tend to occur above the crest of anticlines (e.g. Roberts et al., 2010, Bonini, 2008, 2012), which can trap migrating fluids increasing pore fluid pressures in the structure. A lack of clear imaged anticline related faults seem to suggest that hydrofracturing, at sub-seismic resolution, could be the main mechanism of pipe formation. If this is the case, hydrofractures should occur in the antiform crest and the fluid pipe should be associated with it. Løseth et al. (2011) suggest that, in addition to the resolution problem, when the hydraulic fractures reach the surface a sort of erosive fluid buoyancy starts, cannibalising the formed hydrofractures. This may explain why evidence for hydrofractures are so rarely visible at seismic scale. Therefore, a possibility is that the anticline associated to the last Eocene-Miocene compressive tectonic regional event is affected mostly by fractures that act as precursor to those

fluid pipe rocks but do not evolve into fault with visible vertical displacement. According to all these observations, we hypothesize that, even if brittle structures are apparently absent and not visible in the seismic volume above the anticline, the stresses that controlled fracturing have influenced pipe alignments and their asymmetrical distribution from North to South.

5.3. Evolutionary model

In contrast to similar features described in the literature (e.g. Davies, 2003; Cartwright et al., 2007; Løseth et al., 2009; Cathles et al., 2010; Moss & Cartwright, 2010; Plaza-Favarola et al; 2011; Cartwright & Santamarina, 2015), many of our pipes and fluid escape structures show a variety of intermediate features. Classical pipes generated by the upward migration of hydrocarbon through the stratigraphic sequence can lead (if gas is trapped) to a push down effect, which is not observed in our dataset. Here, the conduits are characterized by an upward deflection, which can be considered a true (non-artifactual) feature (Fig. 5b). This feature is most commonly observed in straight pipe conduits. Such a geometry is typical of mud volcanism/intrusion (Cartwright et al., 2007.

5.3.1. Timing of larger pipes development

The geometrical analysis of the pipes show that the pipe structures mainly terminate at a depth corresponding to a major unconformity (or below it), cutting the stratigraphic sequence. Pipes show clear sediment mobilisation from a deep source that cuts the seal of the Lista reservoir. Sediment mobilization explains the observed pipes internal textures, nonetheless, no diffuse major pockmarks or mud cones/volcanoes are visible on the seabed (except for one possible pockmark) accounting for expulsion of sediment-fluid mixture. We hypothesize that some of the pipes may have fed a mud cone at the palaeo-seabed, but that their evidence have been possibly

deleted by erosion during the formation of the unconformity. Even if no lithostratigraphic wells are available for the Neogene succession to calibrate the younger portion of the stratigraphic sequence (the available well log starts from the Baldar Formation) according to the consideration expressed in section 3.2, we tentatively correlated this unconformity with the INU or LOEMU of Stocker et al. (2002). We therefore suggest that, if present, mud cones at a paleo-seabed could have been eroded during Neogene times, by the deposition of the Miocene erosive contouritic deposits (Shoulders & Cartwright, 2004). This constitutes an upper boundary for the age of these structures, since no pipes propagate above this surface. Furthermore, another temporal limit is represented by the faults: no faults cut the pipe structures, but the pipes in some cases seem to exploit or cut previously formed fault structures (see Figure 6d). We therefore suggest that the fluid escape pipes probably developed in between the formation of the faults and one of the mapped unconformity (corresponding to the LOEMU or INU). This is consistent with the Mio-Pliocene timing of overpressure and sediment remobilisation observed across the entire area of the North Sea

A further consideration can be done on the velocity of those fluid pipes development. The activation and creation of the pipes might have been fast, but probably scattered through time: it is well documented that mud and fluid injection can be a short-term phenomenon, consisting of multiple reactivations of single pipes (e.g., Guliev, 1992; Graue, 2000; Huuse et al., 2010). This is in agreement with the near-middle-far offset partial stack imaging of a selected pipe, showing that two fluid migration mechanisms controlled the pipes evolution, both in space and time: (1) vertical propagation, during the principal initial triggering of the pipes, and possibly further developed later during re-exploitation of the pipes as fluid conduits, and (2) a lateral migration, transferring fluids (with normal amplitude versus offset trend) from the pipe conduit to the surrounding sediments, along permeable pathways driven by Darcy flow behaviour. This mechanism, produced

the ring of horizontal bright amplitude anomalies observed around some of the sectioned pipes (Fig. 7).

5.3.2. An evolutionary model for larger pipes development

According to described line of evidence we hypothesize the following evolutionary model for the development of the larger pipes (Fig. 18). After a primary event, associate to a major overpressure event responsible for the formation of a pipe structure (Fig. 18a) mostly through hydrofracturing (now invisible at the seismic resolution), a secondary (and maybe multiple) phase of fluids flowed into the pipes reactivating the initial triggered pattern and producing some fluid expulsion fading laterally along permeable paths, as testified by lateral brights (Fig. 18b). The two system has probably been active through alternate cycle of fluid overpressure (Fig. 18c). A similar mechanism has been proposed by Bons & Van Milligen (2001), showing that ballistic transport (i.e. hydrofracturing) may play a significant role in sustaining large scale fluid escapes, despite, what remain mostly visible are the diffusive related structures surrounding the conduits and the fluid pipe final conduit . What also appears clear is the relict nature of the pipes that has not been reactivated after the main erosive IMU/INU event. It is worth noting that brights spots detected in some cases above the pipe terminus and in other case above the unconformity are never associated to a geometrical evidence of primary pipe activation (e.g. upward seismic horizon deflection involving fluid migration). This suggest that the upper portion of some pipes (created after the erosion of the unconformity, and developed above it), contain pathway below the seismic resolution, and may have only recently migrated (post the formation of the main pipe structure) through hydrofractures or connected rock porosity (Fig. 18d). Alternatively, the upper portion of the pipes could have developed as trails of stacked brights, afterward connected by hydraulic fracturing. In agreement with the “relict” hypothesis, no pockmarks, except one, are visible at the seabed. This single specific case seems to correspond to an iceberg plough mark. With reference to Judd & Hovland (2007), we believe that this glacial scouring generated instability and micro-fracturing in a portion of unconsolidated sediment thus inducing permeability which created a preferential site for fluid seepage, and in some cases, resulted in the formation of pockmarks.

5.3.3. From small pipes to large pipes: a continuum of processes

In addition to the larger pipes, smaller leakage pipe-like structures do not developed up to the major unconformity (LOEMU or INU) but terminate deeper. These features are of a smaller scale and probably have more similarity to classical blow-out pipes and wipe-out zones (Fig. 6c). Cartwright (2007) and Cartwright & Santamarina (2015) explain how pipes, diapirs and mud volcanoes form from the same genetic mechanisms (hydrofracturing, fluid buoyancy and migration along structural paths) and their forms represent simply the summative effect of different stages and variations along the same evolutionary process. Furthermore, seepage structures emanate from faults and fractures, confirming that at least two families of leakage flow mechanisms are active. One family is related to pre-existing discontinuities (seeps/wipe-out zone and pipes), while the other set is mainly related to hydrofractures that have the ability to cross the stratigraphic sequence including the seal disregarding pre-existing structures. In particular, as shown by many authors (e.g. Berndt, 2005; Løseth et al., 2011; Bonini, 2012) diameter asymmetry can be correlated to discontinuities or alignment along discontinuities such as fault or fractures. On the contrary, cylindrical leakage structures would be driven simply by overpressure and do not need existing discontinuities to propagate upwards; instead, pore fluid pressure results in hydrofracture and the build-up of the conduit (e.g. Davies et al., 2013).

5.4 Consequences on the overburden imaging

The overall imaging suggest that the entire overburden area (Plio-Pleistocene) may still be affected by pocket of overpressured sand/shale units that represent the relics of complex reactivated injection history. This imply that future exploration may take into account the overpressure probably not fully re-equilibrated through time to reduce risk during the main drilling. Moreover, the diffuse presence of large fluid pipe and blow up structures characterized by strong amplitude and impedance anomalies due to the fluid and material trapped within the

conduit will certainly affect a correct lateral characterization of the velocity model. A correct estimation of those lateral velocity may affect a correct "depth" imaging of the overburden and root zones area currently affecting the main reservoir imaging. With this contribution, we added an additional details on the variability and anisotropy driven by the fluid pipe and blow out structures shape and distribution across the seal/overburden area.

6. Conclusive remarks

In this study we have analysed a series of leakage structures from the Loyal Field, by means of a 3D and partial stack seismic investigation. The investigated pipes are located at the top of a buried antiformal high (at the level of the reservoir seal) which likely had high pore fluid pressure due to migration of fluids into the structure. A statistical analysis suggests that southern pipe alignments are roughly orthogonal and parallel to the axis of the broad anticline, which probably acted as a structural trap for the hydrocarbons feeding the pipe system during the late regional compressive Eocene-Miocene event (Sørensen, 2003). The mapped pipes can be divided into two families: (1) pipes following structural discontinuities, and (2) pipes propagating upward (often bypassing the reservoir seal) by hydraulic fracturing, assisted by the buoyancy of a fluidised and mobilised mud-hydrocarbon mixture, rising from a deep source. These pipes seems to have been active between the formation of faults/fractures and polygonal faults and erosion of a Neogene Unconformity (LOEMU, latest Oligocene-Early Miocene, or INU, Miocene-Early Pliocene). Furthermore, after the initial activation of the pipes, minor, secondary and multiphase activation stages are testified by lateral amplitude anomalies and a stacked series of small brights spots above the pipe terminus. AVO analysis through partial stack suggest injected component within the pipe conduits are brine mud/sand rich. These anomalies are partly related to Darcy flow migration of a non-hydrocarbon bearing fluid and secondary gas leakage from the pipe conduit. Even with evidence of secondary

reactivation, the pipe structures are no longer active and can be considered relict evidence of a past mud-fluid mix injection. The described characteristics of the leakage structures reported in this contribution point to multistage formation of pipes within the same evolutionary process, evolving from classical fluid escape pipes to mud cones, and (in our case probably never achieved) bigger mud volcanoes. This continuum is not necessarily a linear evolutionary process but rather require multistage and punctuated cycle of intrusive and diffuse fluid migrations, resulting in a range of evidence of fluid-sediment interaction from the intrusion of mud bodies, to the movement of fluids along discontinuities.

Acknowledgements

We thank an anonymous reviewer for the several constructive comments. The seismic interpretation and image processing was carried out in the SeisLab facility at the University of Aberdeen (sponsored by BG BP and Chevron). Seismic imaging analysis was performed using GeoTeric® (ffA), and analysis of seismic amplitudes was performed in Petrel® 2016 (Schlumberger). We would like to thank the Tuscany PhD Regional program and the Erasmus+ exchange for funding the Aberdeen permanence of one of us (D.M.). Gazprom for supporting A.J PhD., BP for the release of the Loyal field seismic dataset utilized in this research paper and also N.Vanden Beukel (BP) and M. Gorling (BP) and his colleagues for their assistance.

References

Berndt, C. (2005)- *Focused fluid flow in passive continental margins.* Phil. Trans. R. Soc. A , **363**, 55-2871. doi: 10.1098/rsta.2005.1666

Berndt, C., Bunz S., Mienert J.(2003)- *Polygonal fault systems on the mid-Norwegian margin: a long-term source for fluid flow.* In: Van Rensbergen, P., Hillis, R.R., Morley, C.K. (Eds.), Subsurface Sediment Mobilization, Geological Society of London, London, Special Publication, **216**, 283-290. doi: 10.1144/GSL.SP.2003.216.01.18

Bleacher, J. E., Glaze, L. S., Greeley, R., Hauber, E., Baloga, S. M., Sakimoto, S. E., Williams, D.A., Glotch, T. D. (2009)- *Spatial and alignment analyses for a field of small volcanic vents south of Pavonis Mons and implications for the Tharsis province, Mars.* Journal of Volcanology and Geothermal Research,**185-1**, 96-102. http://dx.doi.org/10.1016/j.jvolgeores.2009.04.008

Bitrus, P. R., Iacopini, D., Bond, C. E. (2016)- *Defining the 3D geometry of thin shale units in the Sleipner reservoir using seismic attributes*. Marine and Petroleum Geology, **78**, 405-425. http://dx.doi.org/10.1016/j.marpetgeo.2016.09.020

Bonini, M. (2008)- *Elliptical mud volcano caldera as stress indicator in an active compressional setting (Nirano, Pede-Apennine margin, northern Italy).* Geology, **36(2**), 131-134. doi: 10.1130/G24158A.1

Bonini, M. (2012)- *Mud volcanoes: Indicators of stress orientation and tectonic controls.* Earth-Science Reviews, **115**, 121-152; http://dx.doi.org/10.1016/j.earscirev.2012.09.002

Bons, P. D., & van Milligen, B. P. (2001)- *New experiment to model self-organized critical transport and accumulation of melt and hydrocarbons from their source rocks*. Geology, ***29*-10**, 919-922.

Brown, A. R. (2011)-*Interpretation of three-dimensional seismic data*. Society of Exploration Geophysicists and American Association of Petroleum Geologists.

Brown, K. M. (1990)- *The nature and hydrological significance of mud diapirism and diatremes for accretionary systems.* J. Geophys. Res., **95**, 8969-8982. doi: 10.1029/JB095iB06p08969

Cartwright, J.A. (1994)- *Episodic basin-wide fluid expulsion from geopressured shale sequences in the North Sea basin.* Geology, **22**, 447-450. doi: 10.1130/0091-7613(1994)022<0447:EBWFEF>2.3.CO;2

Cartwright, J.A. & Dewhurst, D.N. (1998)- *Layer-bound compaction faults in fine-grained sediments.* GSA Bulletin, **110-10**; 1242-1257. doi: 10.1130/0016-7606(1998)110<1242:LBCFIF>2.3.CO;2

Cartwright, J. (2007)- *The impact of 3D seismic data on the understanding of compaction, fluid flow and diagenesis in sedimentary basins.* Journal of the Geological Society, **164**, 2007, 881-893. doi: 10.1144/0016-76492006-143

Cartwright, J., Huuse, M., Aplin, A. (2007)- *Seal bypass systems.* AAPG Bulletin, **91-8**, 1141-1166. doi:10.1306/04090705181

Cartwright J. & Santamarina, C. (2015)- *Seismic characteristics of fluid escape pipes in sedimentary basins: Implications for pipe genesis.* Marine and Petroleum Geology, **65**, 126-140. http://dx.doi.org/10.1016/j.marpetgeo.2015.03.023

Cathles, L. M., Su, Z., Chen, D. (2010)- *The physics of gas chimney and pockmark formation, with implications for assessment of seafloor hazards and gas sequestration*. Marine and Petroleum Geology, **27**, 82-91. http://dx.doi.org/10.1016/j.marpetgeo.2009.09.010

Castagna, J.P. (1993)- *Petrophysical imaging using AVO*. The Leading Edge, **12-3**, 172-178. doi: 10.1190/1.1436939

Castagna, J.P & Swan (1997)- *Principles of AVO crossplotting*. The Leading Edge, 16(4), 337-344.

Chopra, S. & Marfurt, K. J. (2007)- *Seismic attributes for prospect identification and reservoir characterization.* Society of Exploration Geophysicists, Tulsa, OK, 456 p. http://dx.doi.org/10.1190/1.9781560801900.fm

Davies, R. J. (2003)- *Kilometer-scale fluidization structures formed during early burial of a deep-water slope channel on the Niger Delta.* Geology, 31-11, 949-952. doi: 10.1130/G19835.1

Davies, R.J., Foulger, G.R., Mathias, S., Moss, J., Hustoft, S., Newport, L. (2013.)- *Reply: Davies et al., 2012. Hydraulic fractures: How far can they go?* Marine and Petroleum Geology, **43**, 519-521. http://dx.doi.org/10.1016/j.marpetgeo.2012.12.008

Dean, K., McLachlan K., Chambers, A. (1999)- *Rifting and the development of the Faeroe–Shetland Basin.* In: Fleet, A.J. & Boldy, S.A.R. (eds) Petroleum Geology of Northwest Europe: Proceedings of the 5th Conference. Geological Society, London, 533-544. doi: 10.1144/0050533

Doré, A.G., Lundin, E.R., Birkeland, Ø., Eliassen, P.E., Jensen, L.N. (1997)- *The NE Atlantic Margin: Implications of late Mesozoic and Cenozoic events for hydrocarbon prospectivity.* Petroleum Geoscience, **3**, 117-131. doi: 10.1144/petgeo.3.2.117

Doré, A.G., Lundin, E.R., Jensen, L.N., Birkeland, Ø., Eliassen, P.E., Fichler, C. (1999)- Principal tectonic events in the evolution of the northwest European Atlantic margin. *In:* Fleet, A.J. & Boldy, S.A.R. (eds) *Petroleum Geology of Northwest Europe: Proceedings of the 5th Conference.* Geological Society, London, 41-61. doi: 10.1144/0050041

Dowdeswell, J. A., & Ottesen, D. (2013)- *Buried iceberg ploughmarks in the early Quaternary sediments of the central North Sea: a two-million year record of glacial influence from 3D seismic data.* Marine Geology, **344**, 1-9. https://doi.org/10.1016/j.margeo.2013.06.019

Graue, K. (2000)- *Mud volcanoes in deepwater Nigeria.* Marine and Petroleum Geology, **17**, 959-974. http://dx.doi.org/10.1016/S0264-8172(00)00016-7

Guliev, I.S. (1992)- *A review of mud volcanism. Translation of the report by: Azerbaijan Academy of Sciences Institute of Geology.* 65pp.

Hansen, J.P.V, Cartwright, J.A., Huuse M., Clausen, O.R. (2005)- *3Dseismic expression of fluid migration and mud remobilization on the Gjallar Ridge, offshore mid-Norway. Basin Research, **17**, 123-139.* doi: 10.1111/j.1365-2117.2005.00257.x

Hustoft, S., Bünz, S., Mienert, J. (2010)- *Three-dimensional seismic analysis of the morphology and spatial distribution of chimneys beneath the Nyegga pockmark field, offshore mid-Norway.* Basin Res. **22**, 465-480. doi: 10.1111/j.1365-2117.2010.00486.x

Huuse, M. & Mickelson, M. (2004)- *Eocene sandstone intrusions in the Tampen Spur area (Norwegian North Sea Quad 34) imaged by 3D seismic data.* Mar. Petrol. Geol., **21**, 141-155. http://dx.doi.org/10.1016/j.marpetgeo.2003.11.018

Huuse, M., Jackson, C.A.-L., Van Rensbergen, P., Davies, R.J., Flemings, P.B., Dixon, R.J., (2010)- *Subsurface sediment remobilization and fluid flow in sedimentary basins: an overview.* Basin Research, **22**, 342-360. doi: 10.1111/j.1365-2117.2010.00488.x

Judd, A.G. & Hovland, M. (2007)- *Seabed Fluid Flow: the Impact on Geology, Biology and the Marine Environment.* Cambridge University Press, Cambridge.

Knutz, P. C. (2010)- Channel structures formed by contour currents and fluid expulsion: significance for Late Neogene development of the central North Sea basin. *In Geological Society, London, Petroleum Geology Conference series*, **7-1**, 77-94. Geological Society of London. doi: 10.1144/0070077

Lamers, E. & Carmichael, S.M.M. (1999)- *The Paleocene deepwater sandstone play West of Shetland*. In: FLEET, A. J. & BOLDY, S. A. R. (eds.) Petroleum Geology of Northwest Europe: Proceedings of the 5th Conference. The Geological Society, London, 645-659. doi: 10.1144/0050645

Leach, H.M., Herbert,N., Los, A., Smith, R. L. (1999)- *The Schiehallion development.* In: FLEET, A. J. & BOLDY, S. A. R. (eds.) Petroleum Geology of Northwest Europe: Proceedings of the 5th conference, 683-692. ©Petroleum Geology '86 Ltd. Published by the Geological Society, London. doi: 10.1144/0050683

Løseth, H., Gading, M., Wensaas, L., (2009)- *Hydrocarbon leakage interpreted on seismic data.* Marine and Petroleum Geology, **26**, 1304-1319. http://dx.doi.org/10.1016/j.marpetgeo.2008.09.008

Løseth, H., Wensaas, L., Arntsen, B, Hanken, N-M, Basire, C, Graue, K (2011)- *1000 m long gas blow-out pipes.* Marine and Petroleum Geology, **28**, 1047-1060.

Lutz, T.M. (1986)- *An analysis of the orientations of large scale crustal structures: A statistical approach based on areal distributions of pointlike features.* Journal of Geophysical Research, **91**, 421-434. doi: 10.1029/JB091iB01p00421

Moss, J.L. & Cartwright, J. (2010)- *3D seismic expression of km-scale fluid escape pipes from offshore Namibia.* Basin Research, **22**, 481-501. doi: 10.1111/j.1365-2117.2010.00461.x

Ostrander, W. J. (1984)- *Plane-wave reflection coefficients for gas sands at non-normal angles of incidence.* Geophysics, **49**, 1637-1648. doi: 10.1190/1.1441571

Plaza-Faverola, A., Bunz, S., Mienert, J. (2011)- *Repeated fluid expulsion through sub seabed chimney offshore Norway in response to glacial cycles*. Earth and Planetary Sciences Letters, **305**, 297-308. doi: 10.1016/j.epsl.2011.03.001

Richardson, K.R., White, R.S., England, R.W., Fruehn, J. (1999)- *Crustal structure east of the Faroe Islands; mapping sub-basalt sediments using wide-angle seismic data.* Petroleum Geoscience, **5**, 161-172. doi: 10.1144/petgeo.5.2.161

Ritchie, J.D., Johnson, H., Quinn, M.F., & Gatliff, R.W. (2008)- *The effects of Cenozoic compression within the Faroe–Shetland Basin and adjacent areas.* In: Johnson H., Doré A. G., Gatliff R.W., Holdsworth R., lundin E.R., Ritchie J.D. (eds). *The Nature and Origin of Compression in Passive Margins.* Geological Society, London, Special Publications, **306**, 121-136. doi: 10.1144/SP306.5

Roberts, D. G., Thomson, M., Mitchener, B., Hossack, J., Carmichael, S. & Bjørseth, H.M. (1999)- *Palaeozoic to Tertiary rift and basin dynamics: mid-Norway to the Bay of Biscay – a new context for hydrocarbon prospectivity in the deep water frontier.* In: FLEET, A. J. & BOLDY, S. A. R. (eds) Petroleum Geology of Northwest Europe: Proceedings of the 5th Conference. The Geological Society, London, 7-40. doi: 10.1144/0050007

Roberts, K. S., Davies, R. J., Stewart, S. A. (2010)- *Structure of exhumed mud volcano feeder complexes, Azerbaijan.* Basin Research, ***22*-4**, 439-451. doi: 10.1111/j.1365-2117.2009.00441.x

Roberts, K. S., Davies, R. J., Stewart, S. A., Tingay, M. (2011)- *Structural controls on mud volcano vent distributions: examples from Azerbaijan and Lusi, east Java.* Journal of the Geological Society, ***168*-4**, 1013-1030. doi: 10.1144/0016-76492010-158

Ross, C. P., & Beale, P. L. (1994)- *Seismic offset balancing*. Geophysics, ***59*-1**, 93-101. https:/doi.org/10.1190/1.1443538

Rutherford, S.R. & Williams, R.H. (1989)- *Amplitude versus offset variation of in gas sand*. Geophysics, **54**, 680-688.

Shoulders, S.J. & Cartwright, J. (2004)- *Constraining the depth and timing of large-scale conical sandstone intrusions. Geology*, **32-8**, 661–664. doi: 10.1130/G20654.1

Smallwood, J.L., Towns, M.J., White, R.S. (2001)- *The structure of the Faroe-Shetland Trough from integrated deep seismic and potential field modelling.* Journal of the Geological Society, London, **158**, 409-412. doi: 10.1144/jgs.158.3.409

Sørensen, A.B. (2003)- *Cenozoic basin development and stratigraphy of the Faroes area.* Petroleum Geoscience, **9,** 189-207. doi: 10.1144/1354-079302-508

Stoker, M.S. (1999)- *Stratigraphic Nomenclature of the UK North West Margin. 3. Mid- to Late Cenozoic stratigraphy.* British Geological Survey, Edinburgh.

Stoker, M.S, Akhurst, M.C, Howe, J.A, Stow, D.A.V. (1998)- *Sediment drifts and contourites on the continental margin off northwest Britain*. Sediment Geol., **115**, 33-51. http://dx.doi.org/10.1016/S0037-0738(97)00086-9

Stoker, M.S., Nielsen, T., van Weering, T.C.E, Kuijpers, A. (2002)- T*owards an understanding of the Neogene tectonostratigraphic framework of the NE Atlantic margin between Ireland and the Faroe Islands.* Marine Geology, **188**, 233-248. http://dx.doi.org/10.1016/S0025-3227(02)00282-7

Stewart, S.A. & Davies, R.J. (2006)- *Structure and emplacement of mud volcano systems in the South Caspian Basin.* AAPG Bulletin, **90-5**,771-786. doi: 10.1306/11220505045

Taner, M. T., Schuelke, James S., O' Doherty, R., Baysal, E. (1994)- *Seismic attributes revisited*. 64th Annual Internat. Mtg., Soc. Expl. Geophys., Expanded Abstracts, **94**, 1104-1106.

Figure Captions

Figure 1. (a,b) Location and structural setting of the study area. The mayor structural elements are reported (structures adapted from Sørensen, 2003 and Ritchie at al., 2008). (c) Loyal Field seismic volume map view reporting the position of the available well log (green circle). Volume location in the 204 and 205 UKCS quadrants is visible in (b). (d) Stratigraphic sequence for the Paleocene-Eocene interval, hosting the Loyal Field and adjoining areas reservoir (Modified from Leach at al., 1999).

Figure 2. Seismic well tie and synthetic seismic generation from well 204/20-3 and 3D seismic data, a) TVD (m) vs TWT (ms) correlation; b) sonic log and density estimated log used for

reflectivity calculation. (c) Reflectivity series; (d) Input and output interval velocity values; (e) Synthetic seismogram generated using Ricker wavelet; (f) Extracted seismic section; (g) Well tops; h) Vertical Seismic profile (VSP) showing average velocity.

Figure 3 (a) Location of the regional seismic section (modified from Stoker et al, 2002) crossing the loyal field and redrawn in (b) showing the main geometrical and stratigraphical relationship of the Eocene-Pliocene units as proposed by Stoker et al (2002). (c) Paleogene and Neogene stratigraphical column of the study area (redrawn after Stoker et al., 2002).

Figure 4. (a) Architecture of the deep portion of the seismic volume. Normal listric faults constituting a tilted block system are well visible. (b) The Top of the Lista Formation surface interpolated by means of 3D mapping. Mounds deforming the surface are well identifiable. (c) Interpretation of a small portion of an inline section depicted by the Trace AGC attribute, showing a channelized body with lateral accretionary seismic packages (LAP'S) in conturitic deposits. (d) Part of the interpolated seabed surface showing iceberg ploughmarks.

Figure 5. (a) "Boosted" Trace AGC inline section showing pipe examples. Whit the term "boost" we refer to the operation of manually rescaling the amplitude values, in a way to augment the amplitude contrast where the signal is poor. In this case it was used to specifically improve the imaging of the seismic volume deep portion. Single and coalescent pipes are visible. In this case, the pipes appear to terminate beneath an erosional unconformity identified as the INU or LOEMU (respectively the Intra Neogene Unconformity or the Latest Oligocene/Early Miocene Unconformity of Stoker et al., 2002). Lateral brights clearly delimitate the pipes conduits. Pipe's root is of difficult interpretation. (b) Close up of a target pipe (interpreted and not interpreted) showing the deflection toward the surface of the seismic horizons. Above the pipe terminus a possible buried pockmark is visible.

Figure 6. Examples of the pipe typology and features mapped in the seismic volume. (a) Portion of a straight pipe showing high deflection of seismic horizons and stacked bright in correspondence of the pipe terminus. (b) Straight and narrow lonely pipe terminating at depth in the subsurface. Lateral brights are present. (c) Diffuse and irregular seeping identifiable as a wipe-out zone. (d) Pipe associated to a structural discontinuity (white arrows). Brights above pipe terminus are visible.

Figure 7. (a) RMS seismic map view of a Paleocene mapped horizon (Surface #13, above the Lista formation see "b") extracted from the overburden above the Lista formation. In purple the low amplitude area representing the sectioned fluid pipe crossing the Surface #13. In green/yallow the distribution of the amplitude anomalies surrounding the fluid pipe structures. (b) Seismic section of the overburden area and position of the seismic Surface #13.

Figure 8. (a) Fluid escape pipe showing lateral migration of fluids, exploiting lateral porosity. Brights indicating presence of fluid fade ahead from the conduit at different heights, indicating scattered activation of the leakage structure. After the primary eruptions secondary drainage events were not able to push the fluids up the paleo-seabed (probably due to the lack of sufficient overpressure) and led these to escape laterally. (b) Two pipes showing a coalescent root.

Figure 9. Graphics plotting pipe axis, measured in the (a) crossline and in the (b) inline. On the right picture it is possible to see how the values were measured along the pipe conduit.

Figure 10. Graphic showing the variation of the Apparent Aspect Ratio (AR_A)**,** which represents the pipe conduit circularity/ellipticity. The more the AR_A value is far from 1, the more the pipe is elliptical.

Figure 11. (a) Graphic showing the measured pipes total lengths, as the sum of different segments (see the figure on the far right). R-TL segment: Root-Top Lista segment, TL-PT segment: Top Lista-

Pipe Terminus segment. (b) Graphic reporting the pipes terminus depth (measured as the PT-SS segment: Pipe Terminus-Seabed Surface segment).

Figure 12. (a) Near- (b) Middle- (c) Far-offset sections extracted from the seismic volume acquired during 2010 and showing the possible presence of hydrocarbon bearing fluid at the pipe terminus (red dashed circle) and of hydrocarbon non-bearing fluid migrating trough porosity away from the pipe conduit (withe dashed ellipse).

Figure 13. Zoomed view of the Partial stacked seismic images from Figure 12. (“a” to “f“ refer to the white dashed ellipse; “g” to “l” refer to the red dashed circle in Fig. 12). (a) Near offset wiggles representation of the CMP traces; (b) medium offset wiggles representation of the CMP traces; (c) far offset wiggles representation of the CMP traces; (d) representation of the Envelope calculated from “a”; (e) representation of the Envelope calculated from “b”; f) representation of the Envelope calculated from “c”; (g) representation of the Envelope calculated from red dashed circle traces Figure 12a; representation of the Envelope calculated from red dashed circle traces Figure 12b; representation of the Envelope calculated from red dashed circle traces Figure 12c. (j). Castagna & Swan (1997) synoptic Intercept-gradient crossplot diagram (for clastic deposit) based on acoustic impedance contrasts. (k) Plot of the gradient and intercept values calculated (using equations “2” and ”3”) using the amplitude extracted from the near to far partial stack in Figure 13 a to c .(l) Plot of the gradient and intercept values calculated (using equations “2” and “3”) using the amplitude extracted from the near to far partial stack represented in “d” to “f”.

Figure 14. (a,b) portion of a time slice Variance attribute delineating the faults and fractures patterns. Convexity of the majority of structures mimics a polygonal fault pattern. Independent fault trace are visible as well. (c) Rose diagram showing the faults and fractures orientation.

Figure 15. (a) the AA' seismic section (imaged by Trace AGC attribute) showing the polygonal faults traces and the graben structure with syn-tectonic sedimentation. Note the correspondence between mounds and faults. For the section orientation see (e). (b) RMS attribute time slice depicting the fluid anomaly (yellow up to red colours) associated to the graben structure. The inset location is indicated in "e". The cross section BB' crossing the graben is visible in "c", where the correspondence between structures and mound is visible again. (d) 3D view of a Trace AGC time intersecting the mapped fault traces. The trace of the BB' cross-section is reported. (e) Map view of the seismic volume reporting the AA' and BB' cross-section traces.

Figure 16. Map view of the seismic volume showing (a) the pipes distribution projected on the Top of Lista Fm surface, and (b) the distribution of the projected fault planes. The trace of the structural high (anticline) axis is reported.

Figure 17. Rose diagram showing the orientation pattern of (a) faults and fractures and (b) to (j) the distribution classes of pipe alignments. Each class contains the frequencies for the various azimuths. A frequency peak for a certain class indicates a possible alignment direction for the pipes. See text for the description of the measurement and statistical procedure. (b) Total dataset (all the pipes were considered) with no weighted frequencies. (c) Total dataset with weighted frequencies. (d) Southern (anticline) cluster (i.e., only the pipes lying above the anticline) with weighted frequencies. (e) Northern cluster (i.e., the remnant pipes, outside the anticline) with weighted frequencies. (f) to (j) Dataset filtered using distance thresholds ranging from 5 to 1 km for the spacing between each pipe.

Figure 18. Schematic cartoon showing the hypothesized evolutionary model for the Loyal Field leakage structures. (a) Development of fractures, normal faults and polygonal faults, above the Lista Fm. (seal); the fluid escape pipes crossed the stratigraphic sequence, creating an upward deflection of the seismic horizons, and possibly reached the paleo-seabed and building up

extrusive mud volcano edifices. (b) Fluid discharge at the seabed terminated, and only minor fluid migration occurred laterally following favourable porosity paths. Such an evolution is presumably due to a decrease in fluid overpressure that prevented the fluids to reach the seabed. (c) The development of the unconformity (possibly the INU or the LOEMU of Stocker et al., 2002) is expected to have erased any evidence of mud cones, which are not visible in the seismic volume. The post-unconformity stratigraphic layers do not register the upward deflection produced by the passage of the fluid-bearing mud, indicating the deactivation of the feeding system. (d) Only some fluids (indicated by brights) are visible at the pipe top, and this probably reveals hydrocarbons that have migrated through porosity or exploiting existing hydrofractures.

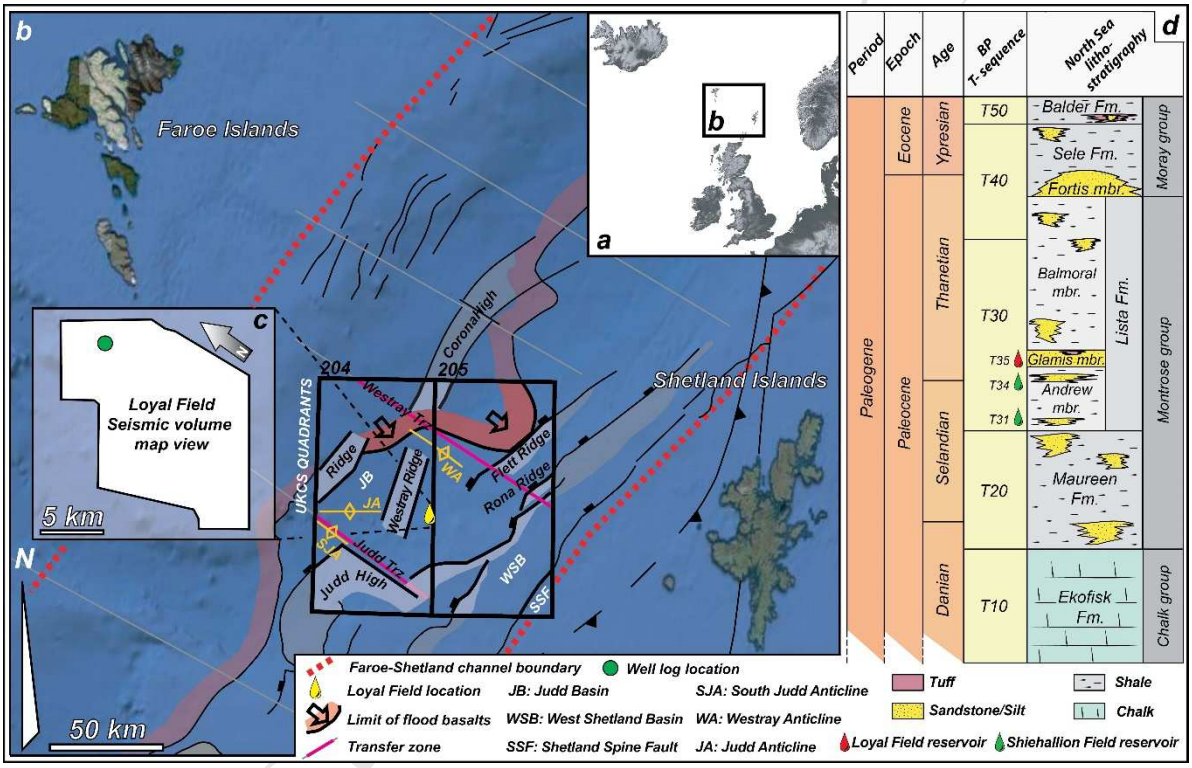

Figure 1 (Revised) - Location, structural setting and stratigraphy

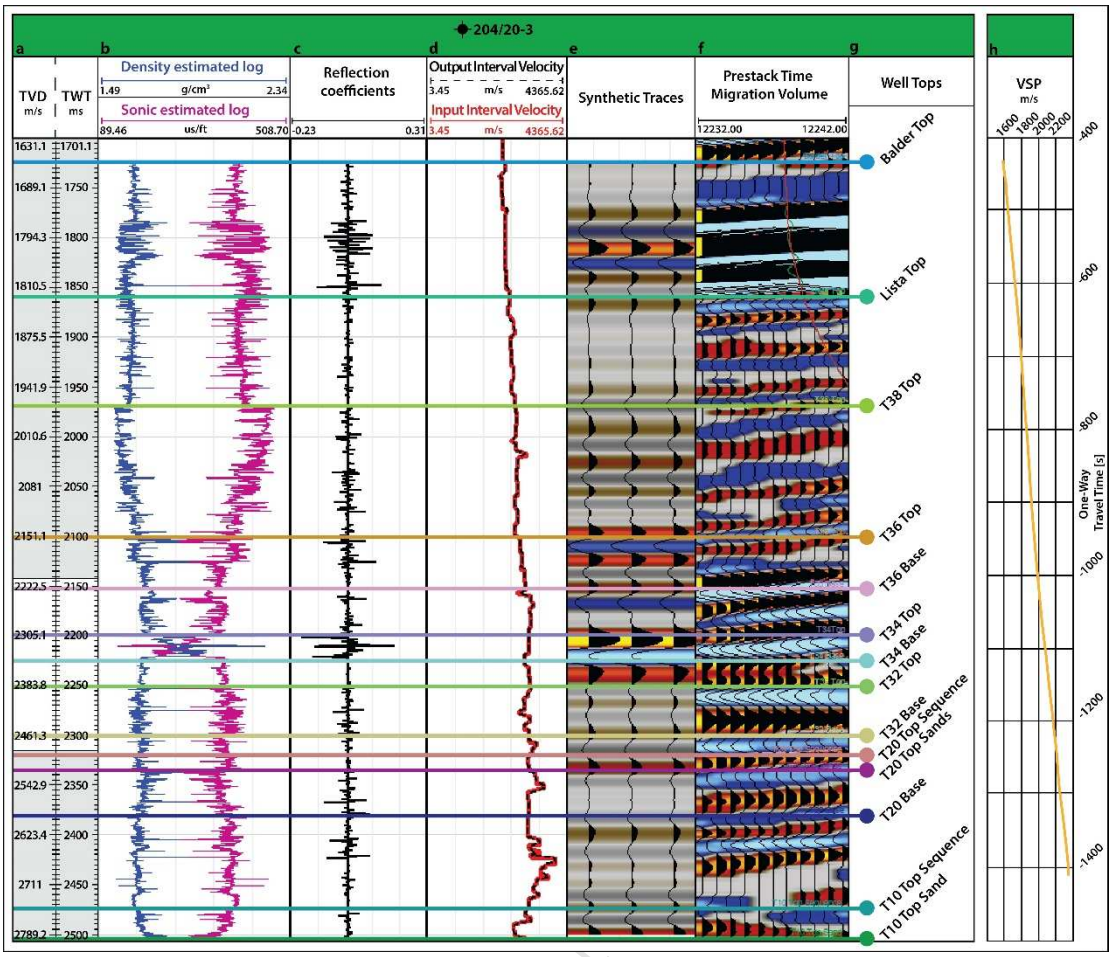

Figure 2 (Revised) - Well log

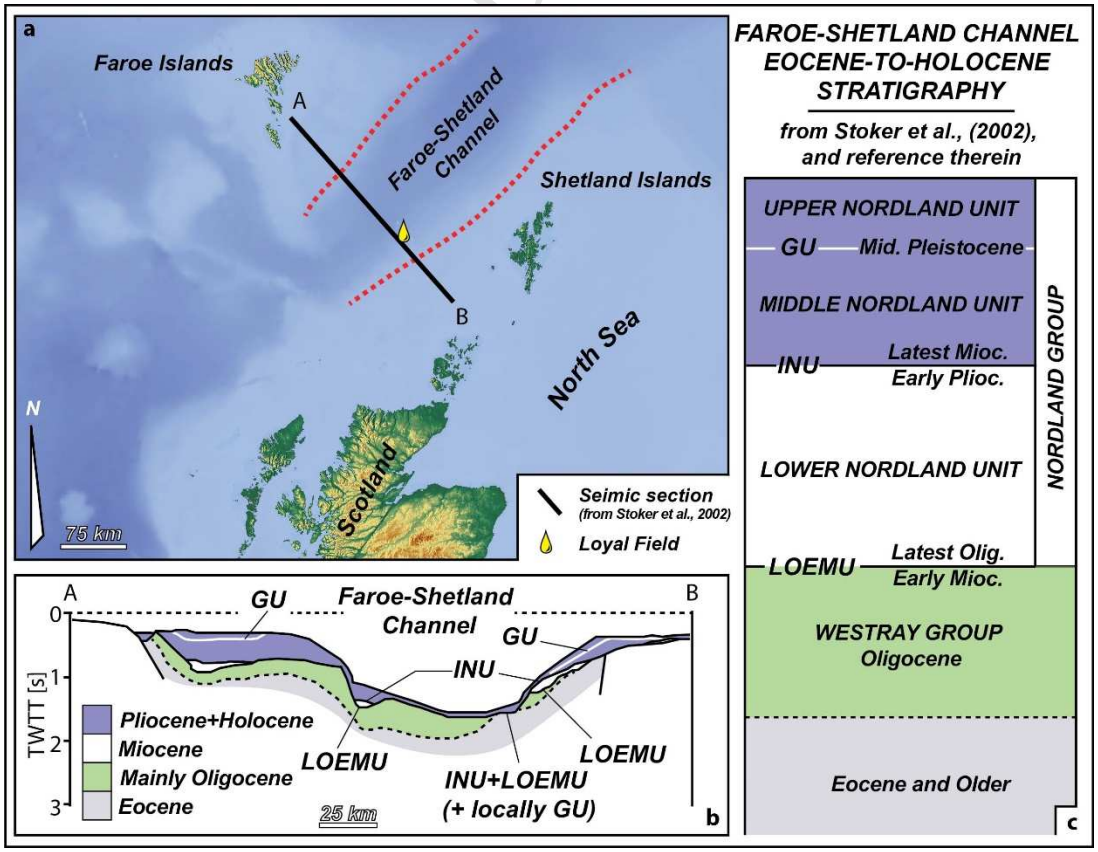

Figure 3 (New) - Regional Seismic cross section and Paleogene-Neogene stratigraphy

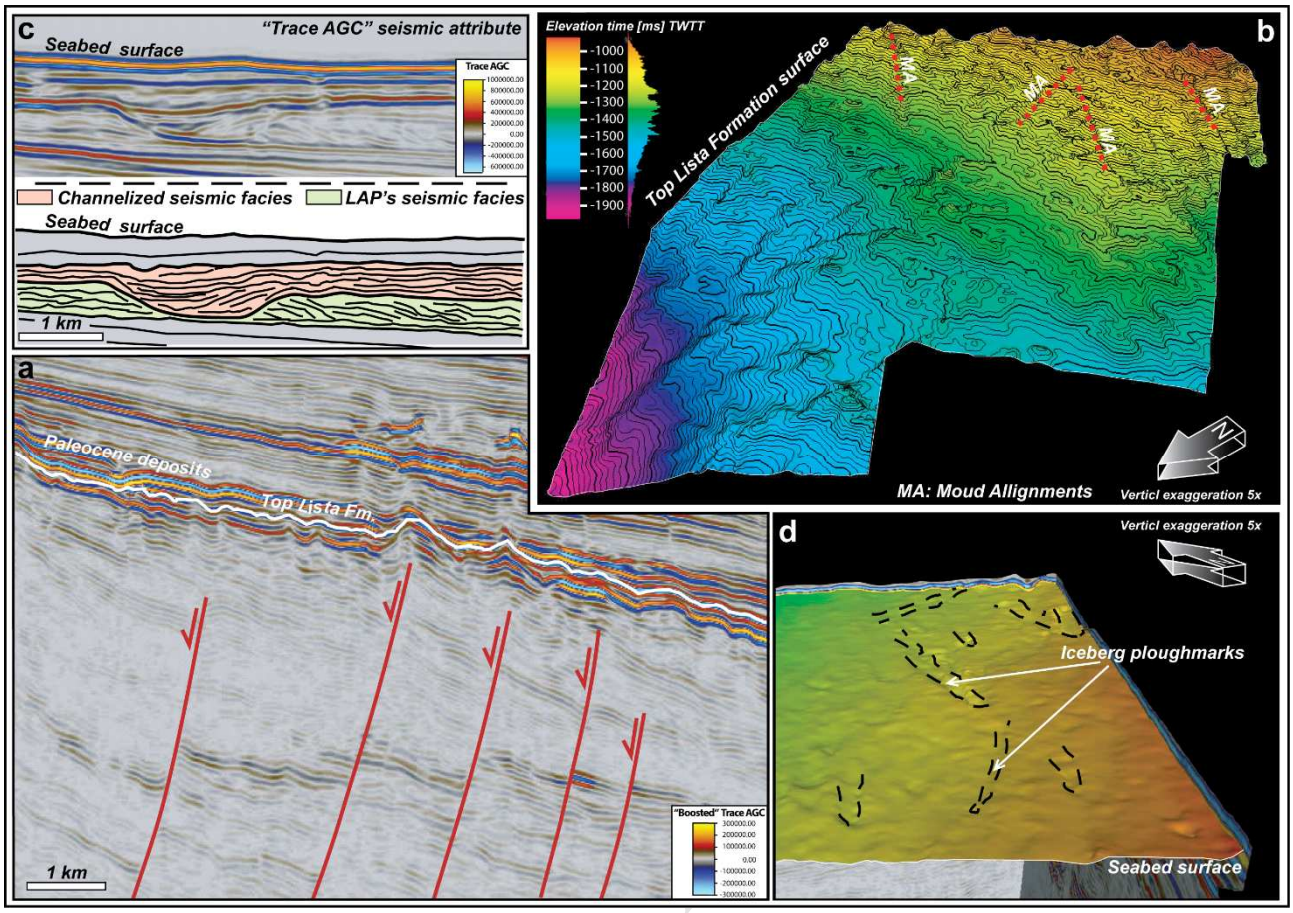

Figure 4 (Revised) - seismic interpretation and mapping

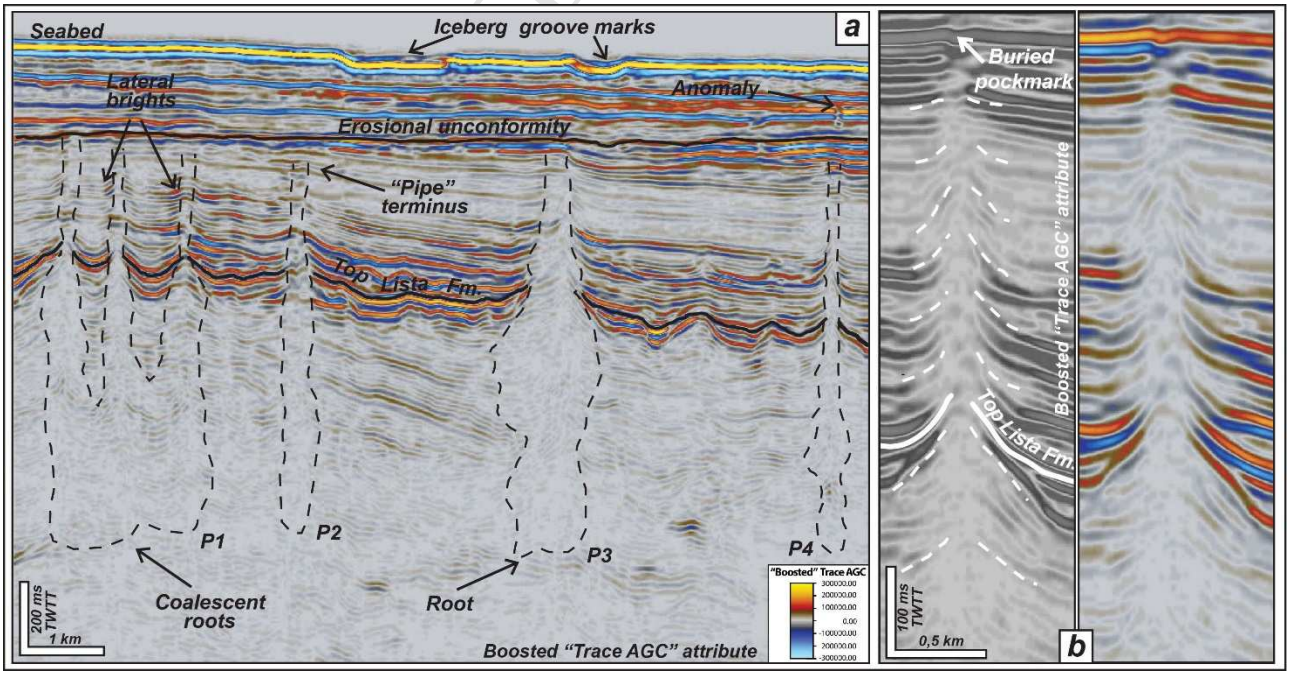

Figure 5 (Revised) - Pipe examples

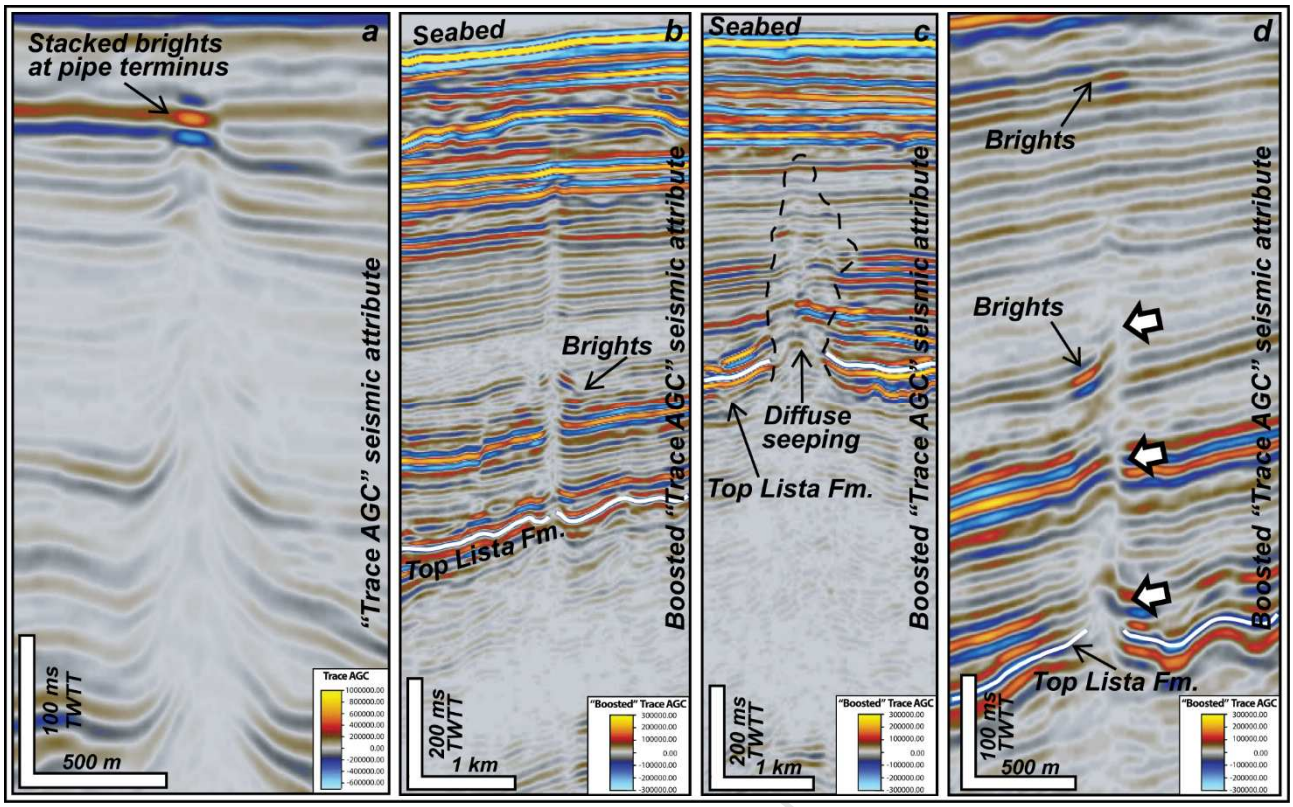

Figure 6 - Pipe examples

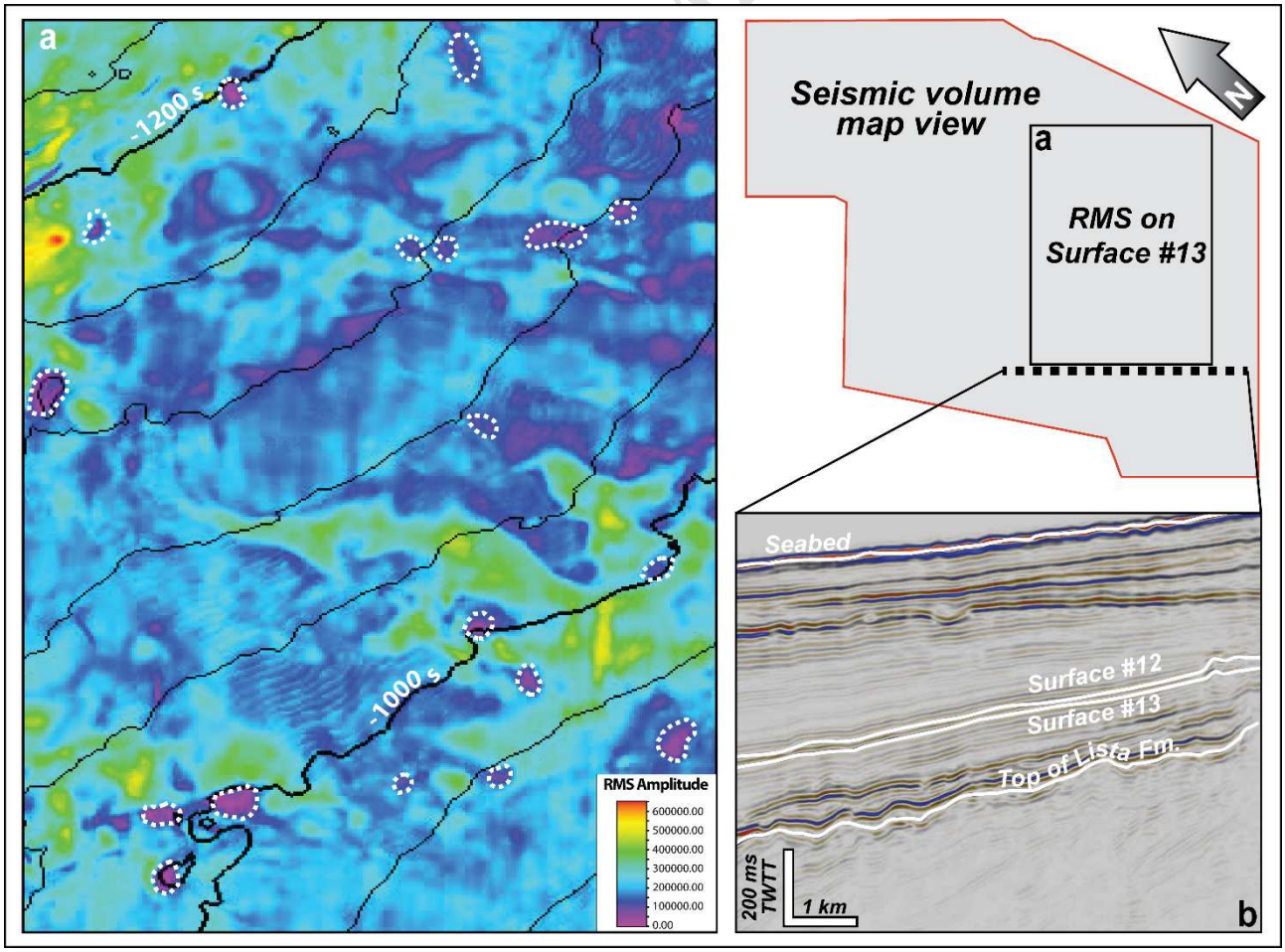

Figure 7 (New) – RMS on target surface

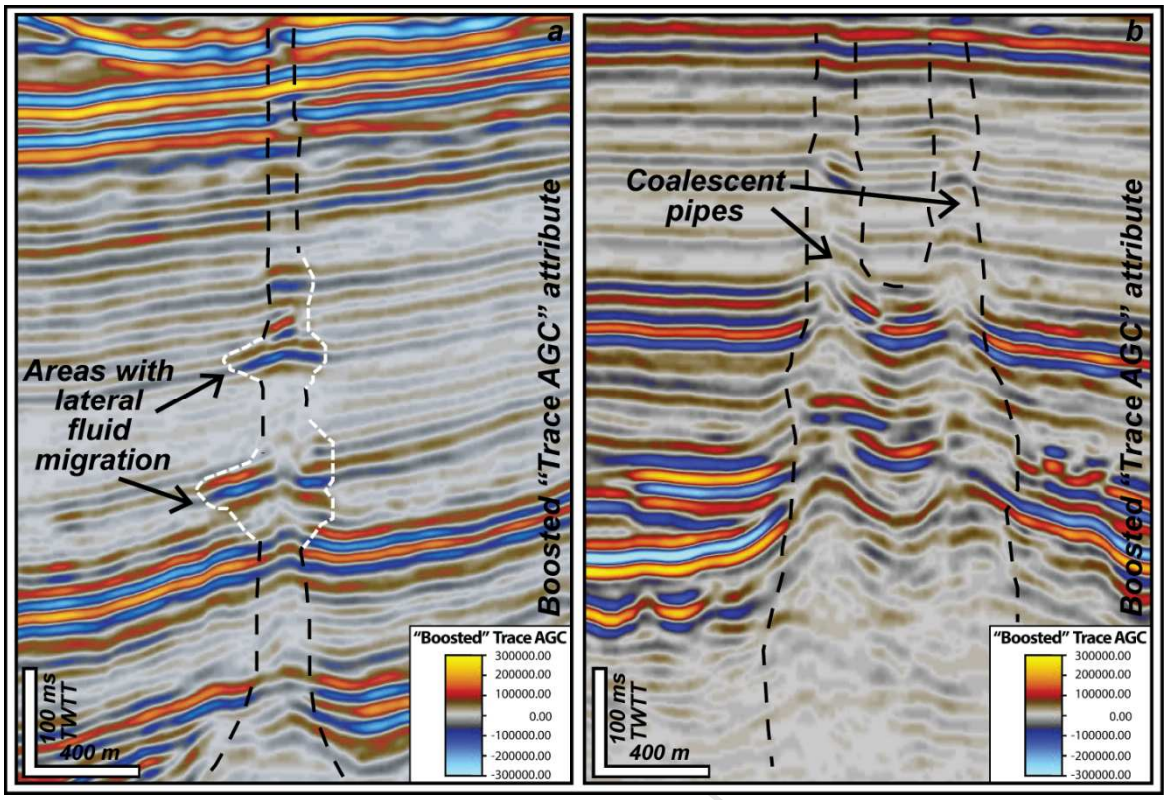

Figure 8 - Lateral migration and coalescent pipes

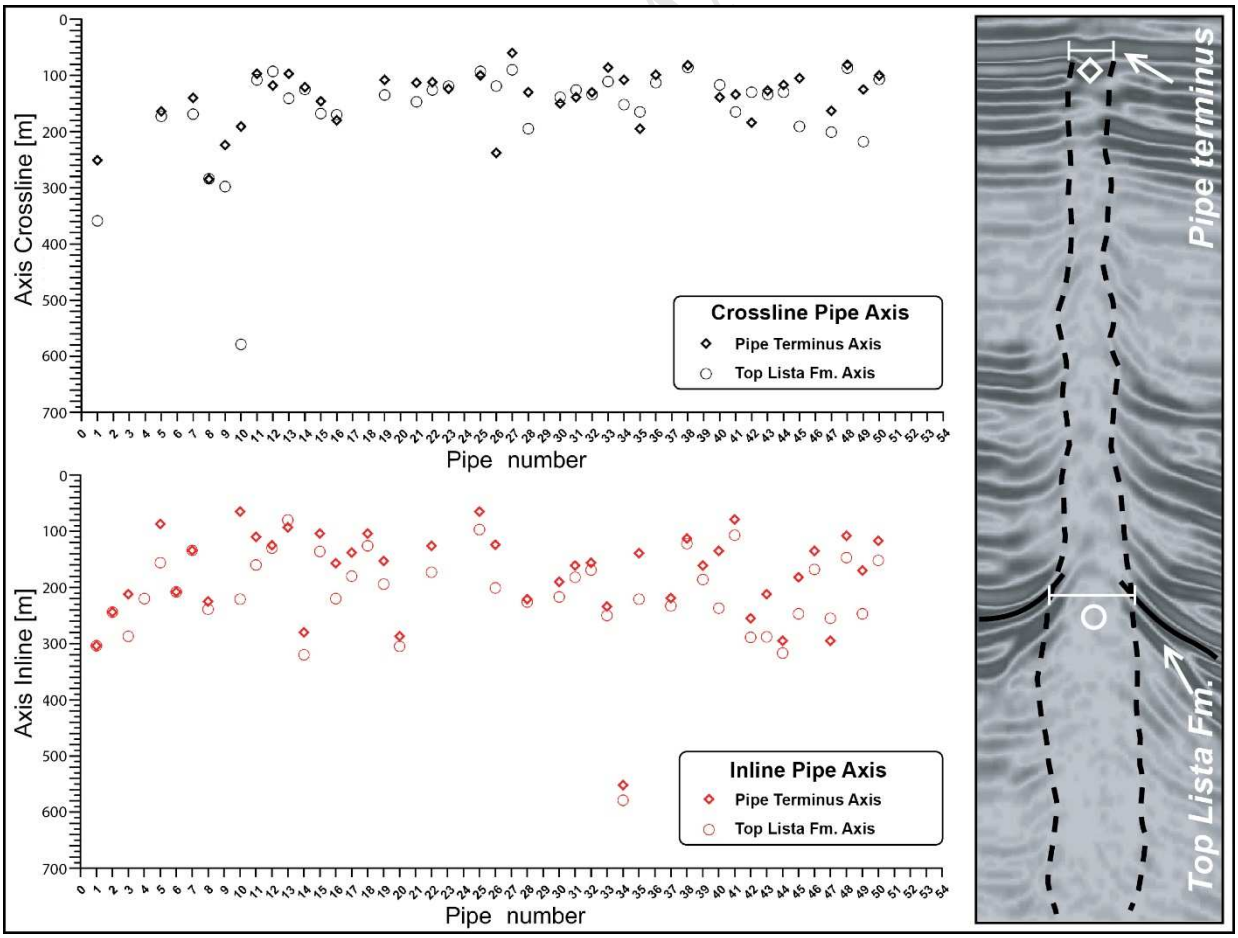

Figure 9 (Revised) - Pipe diameters

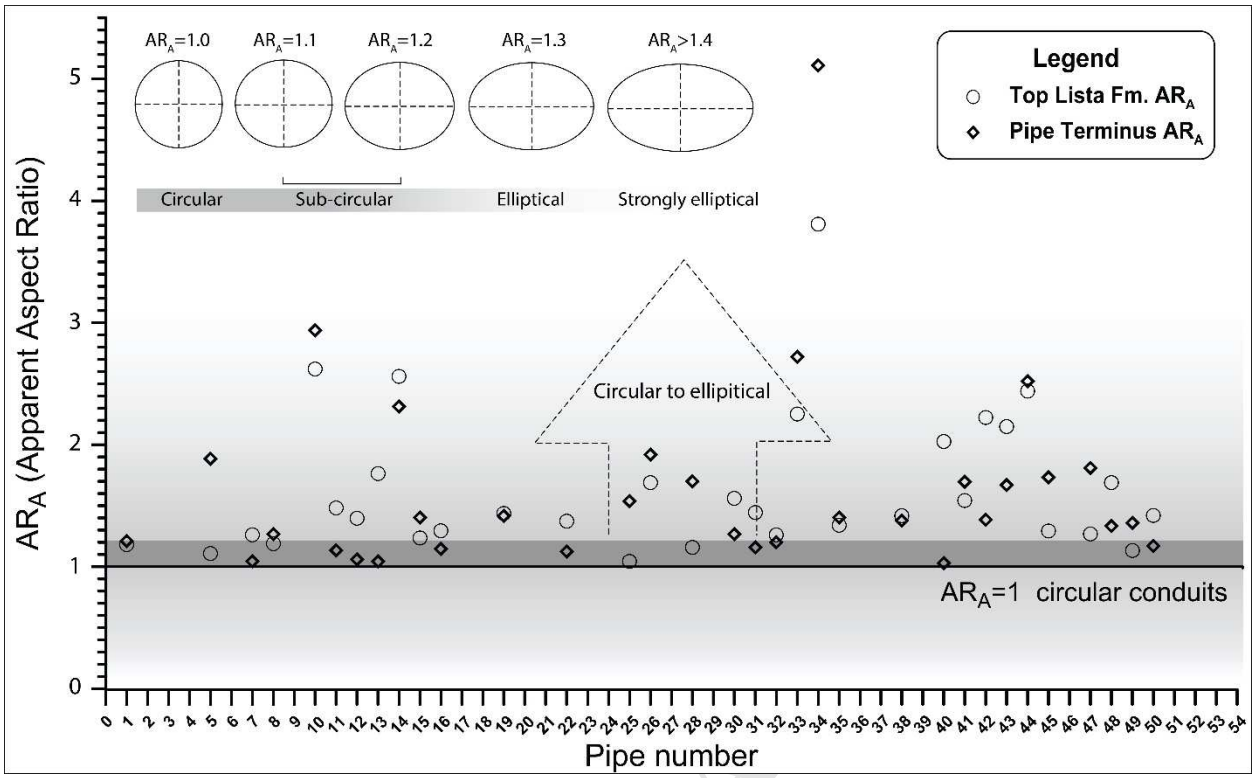

Figure 10 (Revised) - Pipe ellipticity

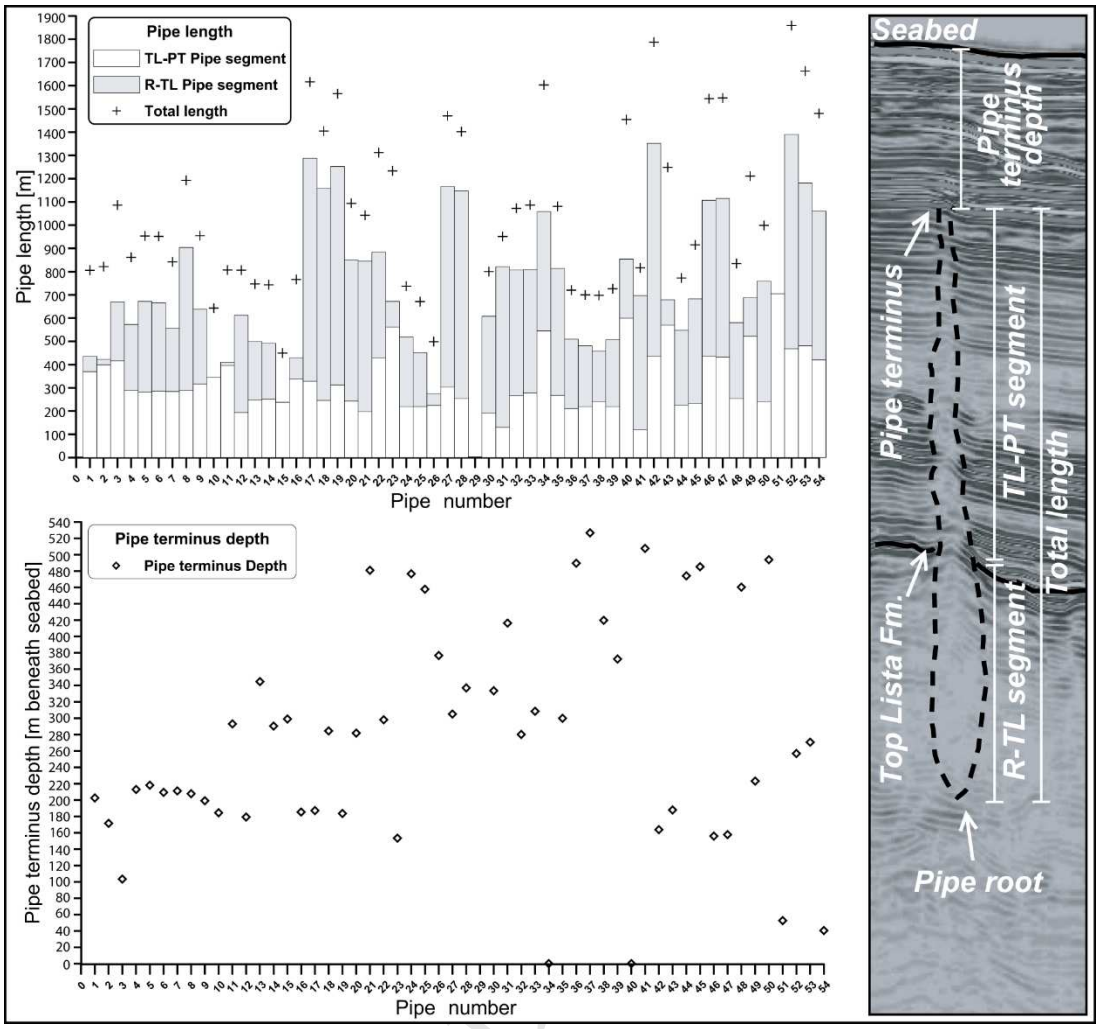

Figure 11 - Pipes length

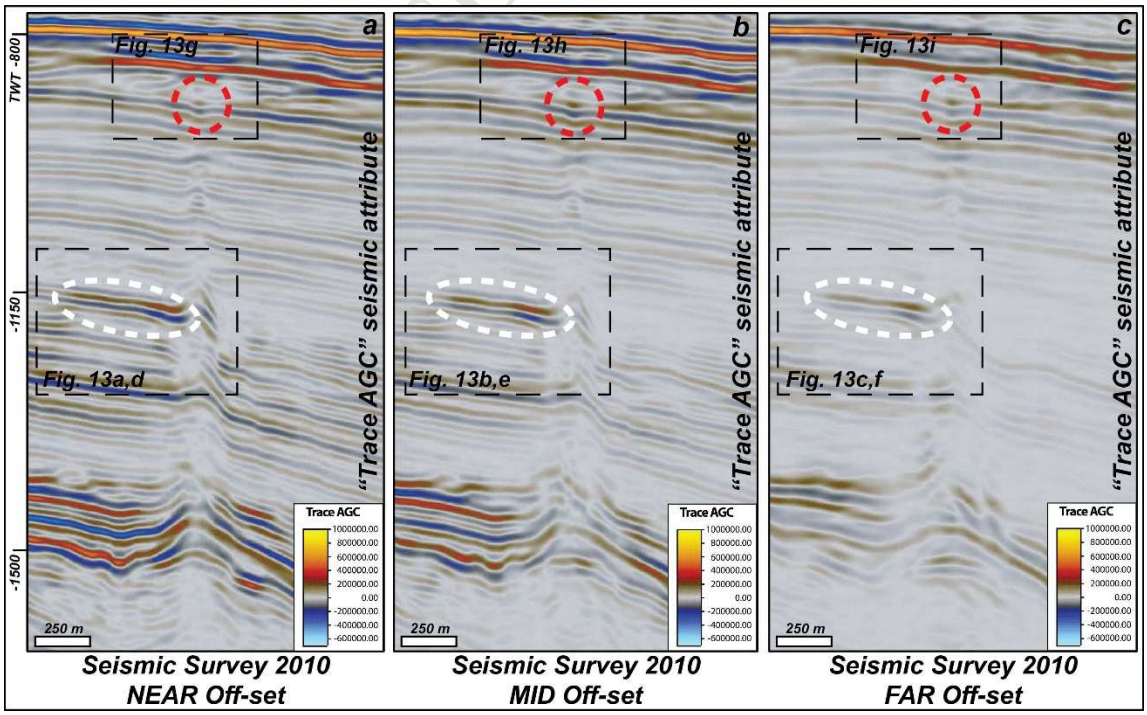

Figure 12 (Revised) - Near-, Mid-, Far-offset analysis

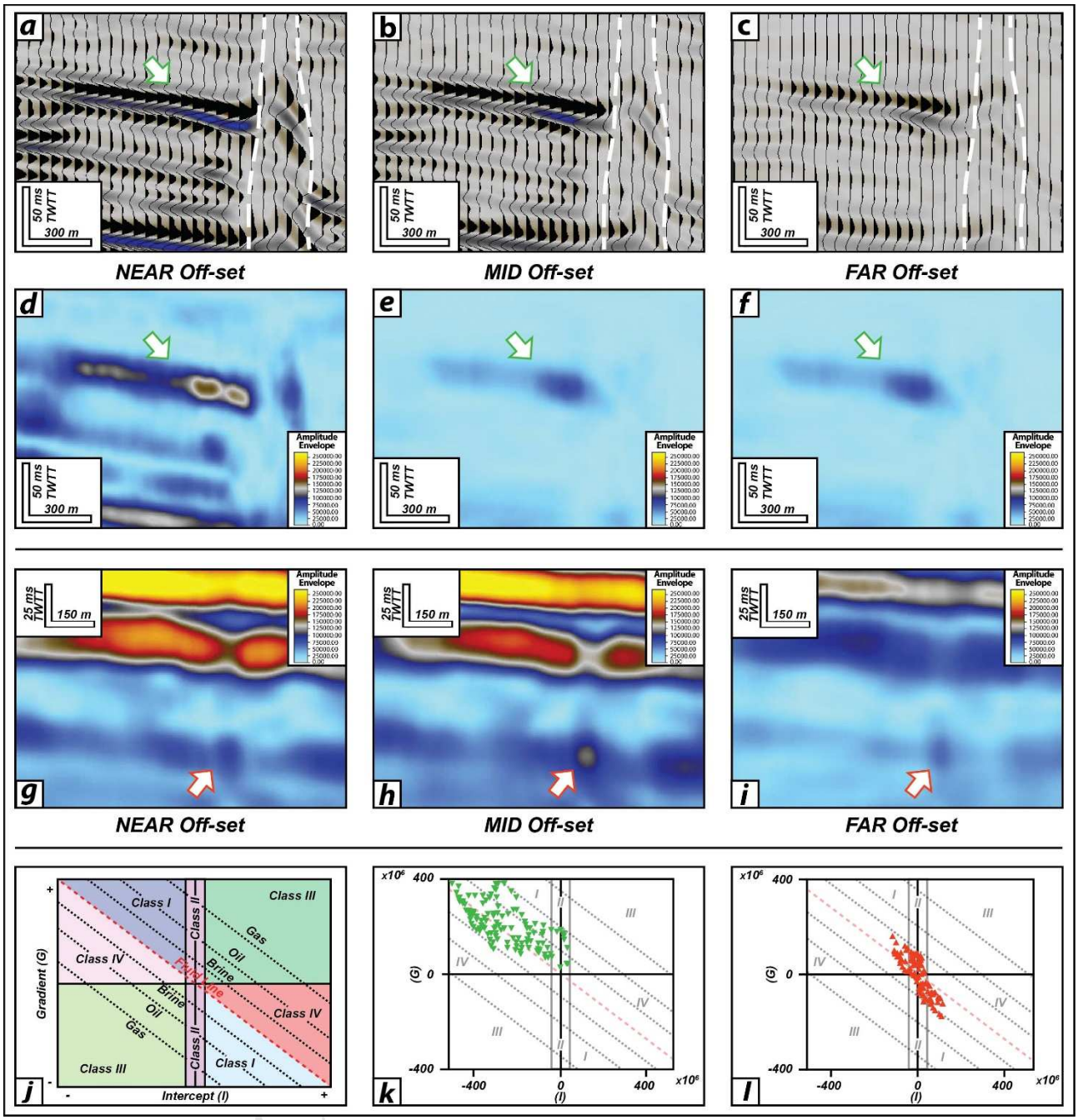

Figure 13 (Revised) - AVO analysis

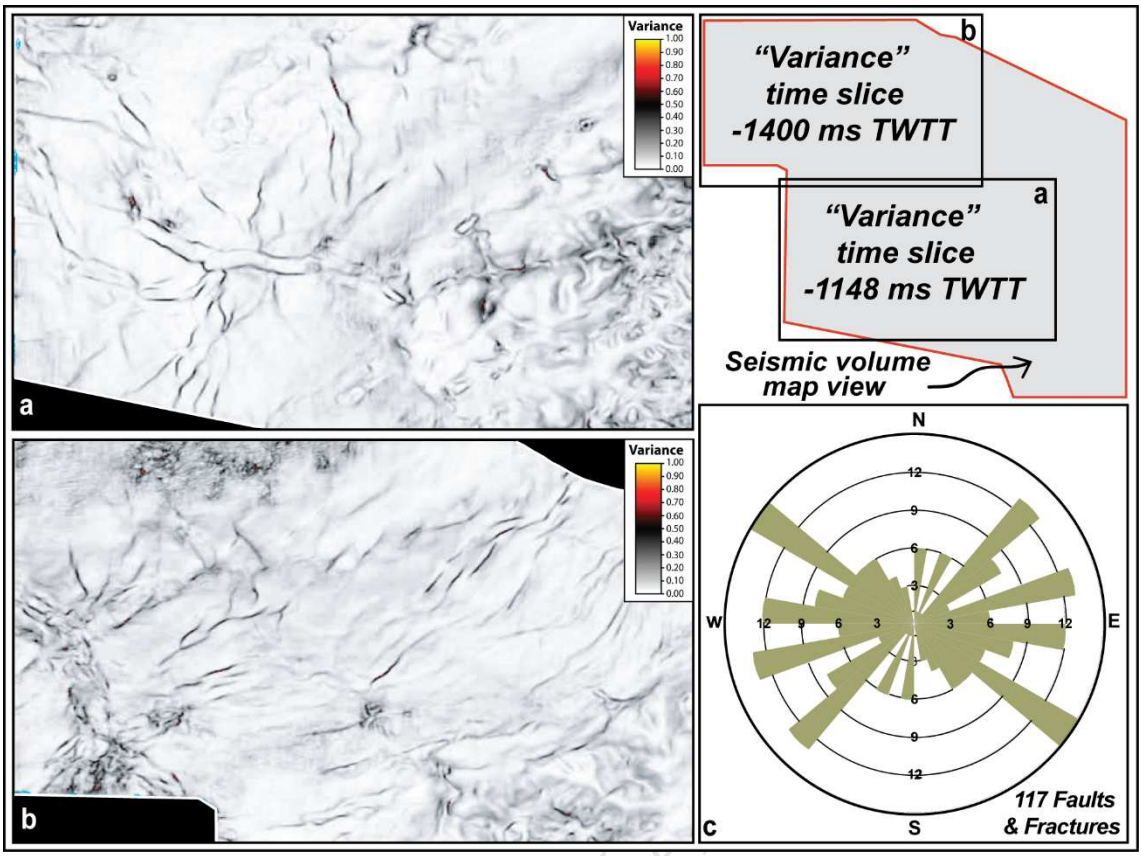

Figure 14 - Structural pattern

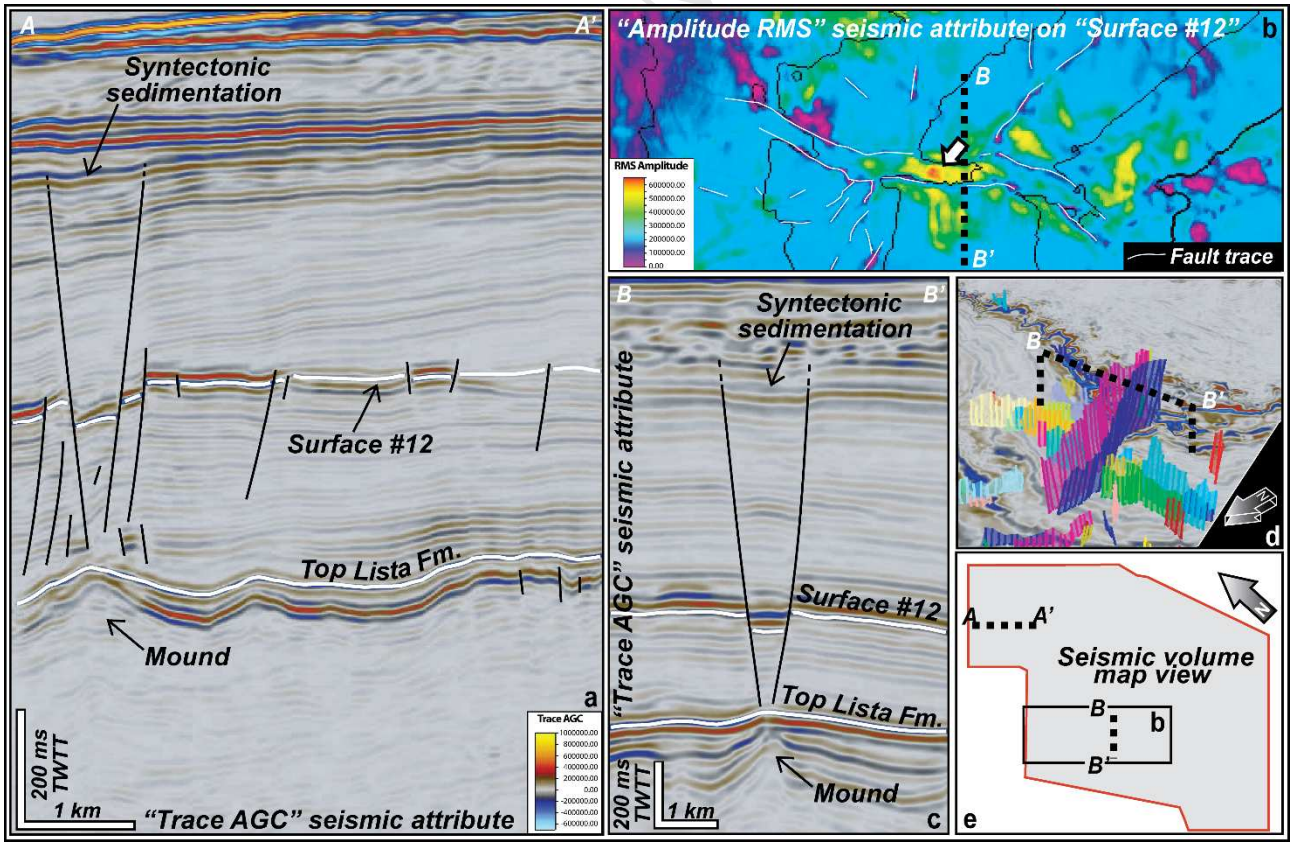

Figure 15 - Faults interpretation

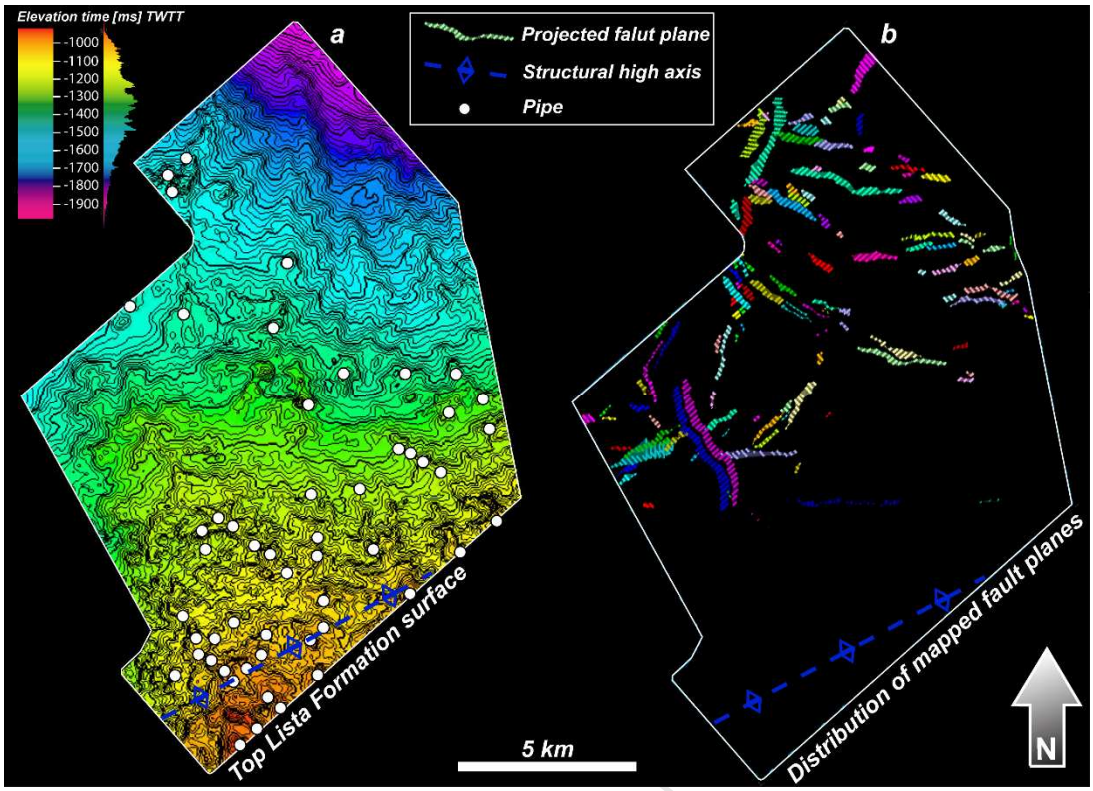

Figure 16 - Pipe location and relation with structures

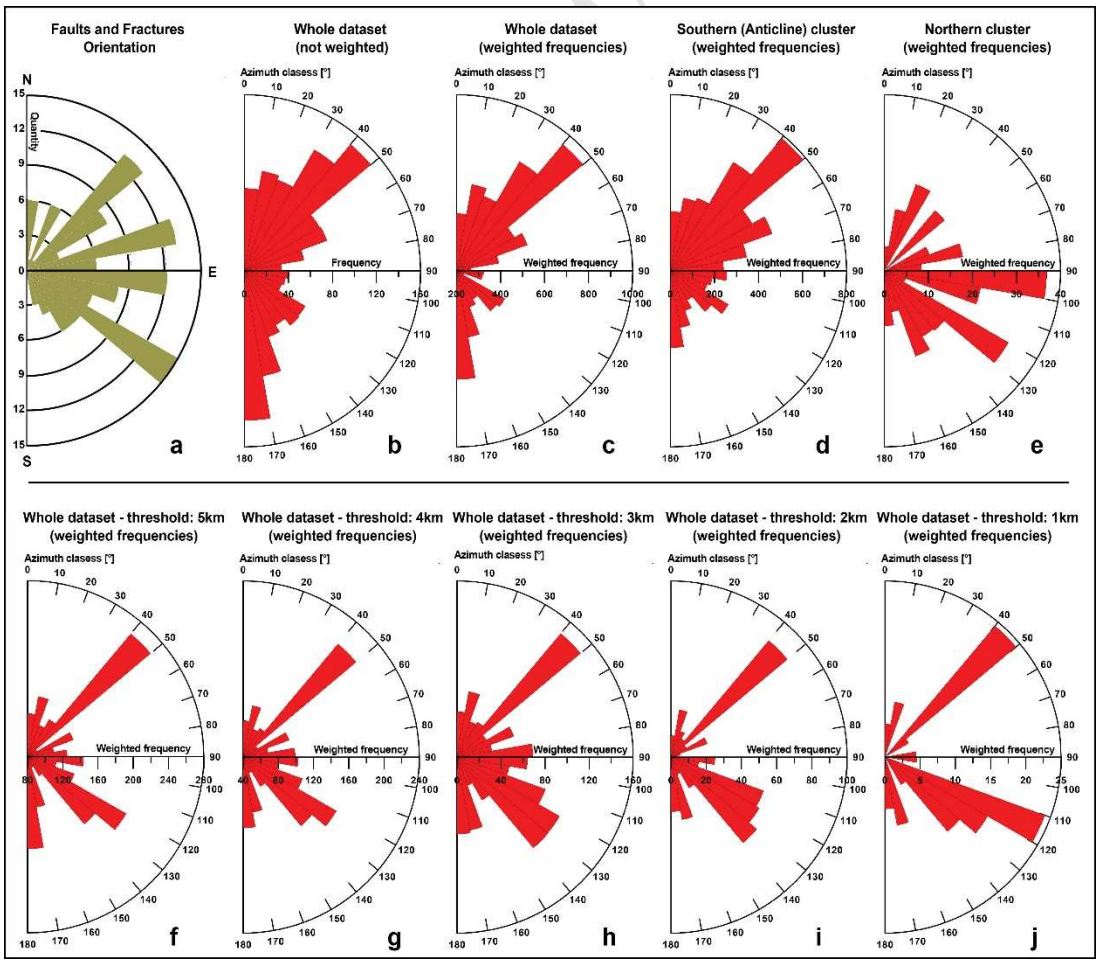

Figure 17 (Revised) - Two points statistics

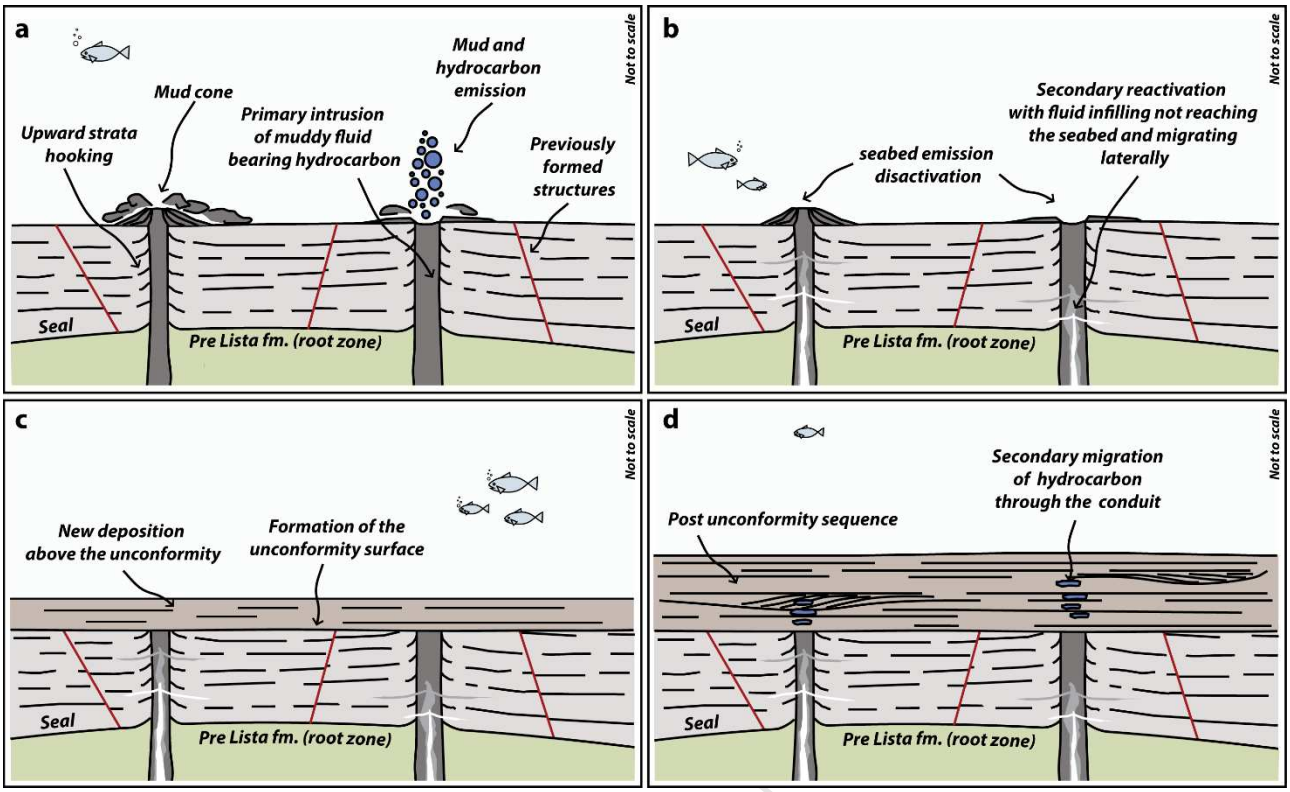

Figure 18 - Evolutionary model

Highlights

- We present a fluid escape pipes interpretation using 3D seismic partial stack data
- Conduits seismic signal response account for mixed fluid-density material intrusion
- Pipes are relicts of Paleogene age resulting by multiphase infilling of mud/fluids
- Pipe intrusion combines hydrofracturing and Darcy flow migration mechanisms